

Effects of Lewis number on vorticity and enstrophy transport in turbulent premixed flames

Nilanjan Chakraborty,^{1,a)} Ilias Konstantinou,¹ and Andrei Lipatnikov²

¹*School of Mechanical and Systems Engineering, Newcastle University, Claremont Road, Newcastle-Upon-Tyne NE1 7RU, United Kingdom*

²*Department of Applied Mechanics, Chalmers University of Technology, Gothenburg 412 96, Sweden*

(Received 12 August 2015; accepted 28 December 2015; published online 20 January 2016)

The effects of Lewis number Le on both vorticity and enstrophy transport within the flame brush have been analysed using direct numerical simulation data of freely propagating statistically planar turbulent premixed flames, representing the thin reaction zone regime of premixed turbulent combustion. In the simulations, Le was ranged from 0.34 to 1.2 by keeping the laminar flame speed, thermal thickness, Damköhler, Karlovitz, and Reynolds numbers unchanged. The enstrophy has been shown to decay significantly from the unburned to the burned gas side of the flame brush in the $Le \approx 1.0$ flames. However, a considerable amount of enstrophy generation within the flame brush has been observed for the $Le = 0.34$ case and a similar qualitative behaviour has been observed in a much smaller extent for the $Le = 0.6$ case. The vorticity components have been shown to exhibit anisotropic behaviour within the flame brush, and the extent of anisotropy increases with decreasing Le . The baroclinic torque term has been shown to be principally responsible for this anisotropic behaviour. The vortex stretching and viscous dissipation terms have been found to be the leading order contributors to the enstrophy transport for all cases, but the baroclinic torque and the sink term due to dilatation play increasingly important role for flames with decreasing Le . Furthermore, the correlation between the fluctuations of enstrophy and dilatation rate has been shown to play an important role in determining the material derivative of enstrophy based on the mean flow in the case of a low Le . © 2016 Author(s). All article content, except where otherwise noted, is licensed under a Creative Commons Attribution (CC BY) license (<http://creativecommons.org/licenses/by/4.0/>). [<http://dx.doi.org/10.1063/1.4939795>]

I. INTRODUCTION

The statistical behaviour of the transport of vorticity and enstrophy is of fundamental importance in the analysis of turbulent fluid motion.^{1–3} The presence of heat release, density variation, and flame normal acceleration in turbulent flames significantly affects the underlying turbulent flow structure and is manifested in flame-generated turbulence⁴ and counter-gradient scalar transport^{5,6} to name a few. While these issues have been the focus of turbulent combustion research for decades (as reviewed elsewhere),⁷ relatively limited effort has been directed to the analysis of the statistical behaviour of vorticity $\vec{\omega}$ and enstrophy Ω transports in turbulent reacting flows.

In non-premixed flames, the alignment of the vorticity vector with local principal strain rates was analysed by Nomura and Elghobashi,⁸ Boratov *et al.*,⁹ and Jaber *et al.*,¹⁰ These analyses demonstrated that vorticity vector $\vec{\omega}$ aligns with the intermediate principal strain rate in non-premixed flames similar to that in non-reacting turbulent flows, but the vorticity vector in non-premixed flames also shows appreciable probabilities of local alignment with the most extensive principal strain rate. The non-premixed flame Direct Numerical Simulation (DNS) data by Boratov *et al.*⁹ have demonstrated that the extent of vorticity alignment with the most extensive principal strain rate increases in regions

^{a)}Email: nilanjan.chakraborty@newcastle.ac.uk. Telephone: +44 0191 208 3570. Fax: +44 0191 208 8600.



where the magnitude of strain rate dominates over the vorticity magnitude. The analysis by Jaber *et al.*¹⁰ indicated that the alignment of vorticity with the intermediate (most extensive) principal strain rate decreases (increases) due to chemical heat release in non-premixed flames, whereas the vorticity vector $\vec{\omega}$ remains mostly perpendicular to the most compressive principal strain rate in both reactive and non-reactive regions of non-premixed turbulent combustion.

In premixed flames, the alignment of vorticity with local principal strain rates has been numerically analysed by Hamlington *et al.*,¹¹ who addressed the thin reaction zones regime combustion. These authors have revealed that vorticity alignment with local principal strain rates in the thin reaction zones regime flames is qualitatively similar to previous findings in the context of non-premixed combustion (i.e., predominant alignment with the intermediate principal strain rate; negligible alignment with the most compressive principal strain rate, and an increased alignment with the most extensive principal strain rate in the heat releasing zone). It was further shown by Hamlington *et al.*¹¹ that vorticity magnitude decays significantly in the burned gas across the flame brush, whereas Treurniet *et al.*¹² demonstrated that vorticity magnitude increases in the burned gas for the flames with high density ratio (or heat release parameter). Lipatnikov *et al.*¹³ analysed the terms of enstrophy and vorticity transport equation for weakly turbulent premixed flames representing the corrugated flamelets regime. While Hamlington *et al.*,¹¹ Treurniet *et al.*,¹² and Lipatnikov *et al.*,¹³ dealt with DNS data, Steinberg *et al.*^{14–17} experimentally investigated the enstrophy field in turbulent premixed flames using cinema-stereoscopic Particle Image Velocimetry (PIV) measurements of rim-stabilised turbulent premixed flames.

Recently, Chakraborty¹⁸ revealed that the global Lewis number Le can significantly affect the vorticity statistics in premixed turbulent combustion. In particular, Chakraborty¹⁸ showed that the statistical behaviour of vorticity alignment with local principal strain rates can be significantly different for the corrugated flamelets regime of combustion with $Le = 1.0$, and for the thin reaction zones regime of combustion with non-unity Lewis number, in comparison to earlier studies.^{8–11,19–28} For example, in the corrugated flamelets regime, and for the cases with high Karlovitz number and low Le , where the most extensive principal strain rate is controlled by the local dilatation rate,¹⁸ the vorticity vector $\vec{\omega}$ predominantly aligns with the intermediate and the most compressive principal strain rates. Such an alignment of the vorticity vector differs from the alignment observed earlier in premixed¹¹ and non-premixed^{8–10} flames with unity Lewis number, or in non-reacting flows.^{19–28}

While each individual species j has its own Lewis number Le_j , in simplified models of molecular transport, the Lewis number of the deficient reactant (fuel or oxidant) is often taken to be the characteristic global Lewis number Le ²⁹ as was done in the aforementioned analysis by Chakraborty.¹⁸ It is worth noting here that alternative methods of assigning a characteristic Lewis number have been proposed based on heat release measurements^{30,31} and mole fractions of the mixture constituents.³²

In the past, the significant effects of characteristic Lewis number Le on various aspects of premixed combustion (e.g., thermo-diffusive instability of laminar flames, burning rate, scalar gradient statistics, and combustion modelling) have been addressed analytically,^{33–36} experimentally,^{37–43} and numerically.^{18,44–53} Various concepts, which have been developed in order to explain such effects in turbulent flames, are reviewed elsewhere.^{54,55} However, the influences of Le on vorticity $\vec{\omega}$ and enstrophy Ω transport are yet to be analysed in detail in the existing literature. In this respect, the main objectives of the present analysis are as follows.

1. To demonstrate the effects of characteristic Lewis number Le on the statistical behaviour of the transport of vorticity $\vec{\omega}$ and enstrophy Ω in turbulent premixed flames.
2. To provide physical explanations for the observed behaviours of the various terms in the vorticity $\vec{\omega}$ and enstrophy Ω transport equation.

The above objectives are met by extracting vorticity $\vec{\omega}$ and enstrophy Ω statistics from DNS data of freely propagating statistically planar turbulent premixed flames with characteristic Lewis number ranging from $Le = 0.34$ to 1.2 .

The rest of the paper is organised as follows. The mathematical background and numerical implementation pertaining to this analysis are presented in Secs. II and III of this paper. Following this, the results are presented and subsequently discussed. The main findings are summarised and conclusions are drawn in Sec. V of this paper.

II. MATHEMATICAL BACKGROUND

The momentum conservation equation for the i th direction is given by

$$\frac{\partial u_i}{\partial t} + u_j \frac{\partial u_i}{\partial x_j} = -\frac{1}{\rho} \frac{\partial p}{\partial x_i} + \frac{1}{\rho} \frac{\partial \tau_{ik}}{\partial x_k}, \quad (1)$$

where u_i is the i th component of velocity, ρ is the gas density, and $\tau_{ij} = \mu(\partial u_i/\partial x_j + \partial u_j/\partial x_i) - (2\mu/3)\delta_{ij}(\partial u_k/\partial x_k)$ is the component of stress tensor, $\mu = \rho\nu$ and ν are dynamic and kinematic viscosities, respectively, and the summation convention applies for the repeated index k . Taking curl of Eq. (1) yields the transport equation of the i th component of vorticity $\omega_i = \varepsilon_{ijk}\partial u_k/\partial x_j$,

$$\frac{\partial \omega_i}{\partial t} + u_k \frac{\partial \omega_i}{\partial x_k} = \underbrace{\omega_k \frac{\partial u_i}{\partial x_k}}_{t_{1i}} - \underbrace{\varepsilon_{ijk} \frac{1}{\rho^2} \frac{\partial \rho}{\partial x_j} \frac{\partial \tau_{kl}}{\partial x_l}}_{t_{21i}} + \underbrace{\frac{\varepsilon_{ijk}}{\rho} \frac{\partial^2 \tau_{kl}}{\partial x_j \partial x_l}}_{t_{22i}} - \underbrace{\omega_i \frac{\partial u_k}{\partial x_k}}_{t_{3i}} + \underbrace{\frac{\varepsilon_{ijk}}{\rho^2} \frac{\partial \rho}{\partial x_j} \frac{\partial p}{\partial x_k}}_{t_{4i}}. \quad (2)$$

The term t_{1i} on the right hand side of Eq. (2) is the i th component of the vortex-stretching term. The i th component of the viscous torque term t_{21i} arises due to the misalignment between the gradients of viscous stress and density and vanishes in constant-density flows. The i th component of term t_{22} is responsible for the diffusion of vorticity and is equal to $\nu\partial^2\omega_i/\partial x_j\partial x_j$ in constant-density flows or in the case of a constant μ (as assumed in the current analysis). The fourth term on the right hand side of Eq. (2) (i.e., i th component of term t_3) is responsible for vorticity destruction by dilatation, whereas the last term on right hand side of Eq. (2) (i.e., i th component of term t_4) is responsible for baroclinic effects arising from the misalignment of the density and pressure gradients. Both term t_3 and t_4 vanish in constant-density flows.

Multiplying ω_i both sides of Eq. (2) yields the transport equation of enstrophy $\Omega = \omega^2/2 = \omega_i\omega_i/2$ (Ref. 13),

$$\frac{\partial \Omega}{\partial t} + u_k \frac{\partial \Omega}{\partial x_k} = \underbrace{\omega_i\omega_k \frac{\partial u_i}{\partial x_k}}_{T_1} - \underbrace{\varepsilon_{ijk}\omega_i \frac{1}{\rho^2} \frac{\partial \rho}{\partial x_j} \frac{\partial \tau_{kl}}{\partial x_l}}_{T_{21}} + \underbrace{\frac{\varepsilon_{ijk}\omega_i}{\rho} \frac{\partial^2 \tau_{kl}}{\partial x_j \partial x_l}}_{T_{22}} - \underbrace{2\frac{\partial u_k}{\partial x_k} \Omega}_{T_3} + \underbrace{\varepsilon_{ijk} \frac{\omega_i}{\rho^2} \frac{\partial \rho}{\partial x_j} \frac{\partial p}{\partial x_k}}_{T_4}. \quad (3)$$

On Reynolds averaging Eq. (3) provides (Ref. 13)

$$\frac{\partial \bar{\Omega}}{\partial t} + u_k \frac{\partial \bar{\Omega}}{\partial x_k} = \underbrace{\overline{\omega_i\omega_k \frac{\partial u_i}{\partial x_k}}}_{T_I} - \underbrace{\overline{\varepsilon_{ijk}\omega_i \frac{1}{\rho^2} \frac{\partial \rho}{\partial x_j} \frac{\partial \tau_{kl}}{\partial x_l}}}_{T_{II}} + \underbrace{\overline{\frac{\varepsilon_{ijk}\omega_i}{\rho} \frac{\partial^2 \tau_{kl}}{\partial x_j \partial x_l}}}_{T_{III}} - \underbrace{\overline{2\frac{\partial u_k}{\partial x_k} \Omega}}_{T_{IV}} + \underbrace{\overline{\varepsilon_{ijk} \frac{\omega_i}{\rho^2} \frac{\partial \rho}{\partial x_j} \frac{\partial p}{\partial x_k}}}_{T_V}, \quad (4)$$

where \bar{Q} indicates the Reynolds averaged value of a general quantity Q . The term T_I is the vortex stretching contribution to the mean enstrophy $\bar{\Omega}$ transport, whereas the term T_{II} is the average of the scalar product of two vectors, the vorticity and the viscosity torque. The term T_{III} , which reads $\overline{\nu\omega_i(\partial^2\omega_i/\partial x_j\partial x_j)} = \overline{\nu\partial^2\Omega/\partial x_j^2} - \overline{\nu(\partial\omega_i/\partial x_j)(\partial\omega_i/\partial x_j)}$ if the dynamic viscosity is constant, represents the combined action of molecular diffusion and dissipation of the mean enstrophy $\bar{\Omega}$. These two sub-terms can be of the same order of magnitude for small values of turbulent Reynolds number, whereas the dissipation sub-term (i.e., $-\overline{\nu(\partial\omega_i/\partial x_j)(\partial\omega_i/\partial x_j)}$) dominates for high values of turbulent Reynolds number. The term T_{IV} is responsible for the dissipation of enstrophy due to dilatation. The term T_V is the baroclinic torque term which arises due to misalignment between pressure and density gradients. The statistical behaviour of these terms will be discussed in detail in Section IV of this paper.

III. NUMERICAL IMPLEMENTATION

As the current analysis focuses on the effects of characteristic Lewis number Le on vorticity and enstrophy transport in isolation, a simple one-step chemistry has been used for the purpose of computational economy following several previous analyses.^{44–52} A well-known compressible code called SENGAS⁵⁶ has been used for the DNS simulations where the standard conservation equations

of mass, momentum, energy, and species are solved in non-dimensional form. The dimensionless forms of the conservation equations are presented in [Appendix A](#). The simulation domain is taken to be a cube of size $24.1\delta_{th} \times 24.1\delta_{th} \times 24.1\delta_{th}$, where $\delta_{th} = (T_{ad} - T_0) / \max |\nabla \hat{T}|_L$ is the thermal flame thickness with T_0 , T_{ad} , and \hat{T} being the unburned gas, adiabatic flame, and instantaneous dimensional temperatures, respectively, and the subscript ‘‘L’’ refers to the unstrained laminar flame condition. A uniform Cartesian grid of $230 \times 230 \times 230$ has been used to discretise the simulation domain, which ensures about 10 grid points within δ_{th} . The spatial derivatives for the internal grid points are evaluated using the 10th order central difference scheme and the order of differentiation drops gradually to a one-sided 2nd order scheme at the non-periodic boundaries. A low storage third order explicit Runge-Kutta scheme⁵⁷ is used for explicit time advancement. The turbulent velocity fluctuations are initialised using a pseudo-spectral method⁵⁸ using the Bachelor-Townsend spectrum.⁵⁹ The scalar field is initialised by an unstrained planar laminar flame solution. The initial values of root-mean-square value of turbulent velocity fluctuation normalised by the unstrained laminar burning velocity u'/S_L , integral length scale normalised by the unstrained laminar flame thickness ratio l/δ_{th} , Damköhler number $Da = lS_L/u'\delta_{th}$, and Karlovitz number $Ka = (u'/S_L)^{1.5}(l/\delta_{th})^{-0.5}$ are 7.5, 2.45, 0.33, and 13.2, respectively. These values of u'/S_L , l/δ_{th} , Da , and Ka represent the thin reaction zones regime combustion according to the regime diagram by Peters.⁶⁰ A single value of heat release parameter $\tau = (T_{ad} - T_0)/T_0 = 4.5$ was set in all studied cases, whereas the Lewis number was varied, i.e., $Le = 0.34, 0.6, 0.8, 1.0$, and 1.2 , with S_L and δ_{th} being kept unchanged by varying the pre-exponential factor in the expression for the reaction rate. The five cases characterized with these five Le will be referred to as cases A-E, respectively. Standard values are taken for Prandtl number Pr , ratio of specific heats $\gamma = c_p/c_v$ and the Zeldovich number $\beta = T_{ac}(T_{ad} - T_0)/T_{ad}^2$ (i.e., $Pr = 0.7$, $\gamma = 1.4$, $\beta = 6.0$), where T_{ac} is the activation temperature. The flame Mach number $Ma = S_L/(\gamma RT_0)^{0.5}$ is taken to be 0.014 for all cases with R being the gas constant. All the simulations have been carried out for a chemical time scale $t_{chem} = \delta_{th}/S_L$, which corresponds to about 3.34 initial integral eddy turnover times (i.e., $t_{chem} = 3.34l/u'$) for the cases considered here. The value of u'/S_L decayed by 50% ahead of the flame, whereas l/δ_{th} increased by a factor of 1.7 when the statistics were extracted. The simulation time used in the current analysis remains comparable to several previous analyses,^{61–67} which have contributed significantly to the fundamental understanding of turbulent reacting flows in the past.

The Reynolds/Favre averaged values have been calculated by ensemble averaging the relevant quantities in transverse directions (i.e., $x_2 - x_3$ planes). The statistical convergence of the averaged quantities has been assessed by comparing the corresponding values obtained using half of the sample size in the transverse directions using a distinct half of the domain, with those obtained based on full sample size. Both the qualitative and quantitative agreements between these sets of values are found to be satisfactory, and only the results obtained based on full sample size will be presented here for the sake of conciseness.

In premixed flames, the species field is often characterised in terms of a reaction progress variable c , which increases from 0.0 in unburned gases to 1.0 in fully burned products. The reaction progress variable c can be defined in terms of a suitable reactant (product) mass fraction Y_R (Y_P) in the following manner: $c = (Y_{R0} - Y_R)/(Y_{R0} - Y_{R\infty})$ ($c = (Y_P - Y_{P0})/(Y_{P\infty} - Y_{P0})$). The statistically planar flames propagate in the negative x_1 -direction for all cases considered here so the Favre averaged reaction progress variable \bar{c} remains a unique function of x_1 . Thus, all the Reynolds averaged quantities are plotted as a function of \bar{c} for all cases considered here in [Sec. IV](#) of this paper.

IV. RESULTS AND DISCUSSION

The distributions of normalised vorticity magnitude $\sqrt{\omega_i\omega_i} \times \delta_{th}/S_L$ in the central $x_1 - x_3$ mid-plane at $t = \delta_{th}/S_L$ for different Lewis number cases are shown in [Fig. 1](#) where the contours of c from 0.1 to 0.9 (left to right) are superimposed on the vorticity magnitude field. It can be seen from [Fig. 1](#) that the wrinkling of c isosurfaces increases with decreasing Le , which can be quantified by the normalised turbulent flame surface area A_T/A_L , which is listed in [Table I](#) for the cases considered here at the time the statistics were taken. The flame surface area has been evaluated using the volume integral $A = \int_V |\nabla c| dV$ for both turbulent and laminar flame cases (shown with subscripts T and L,

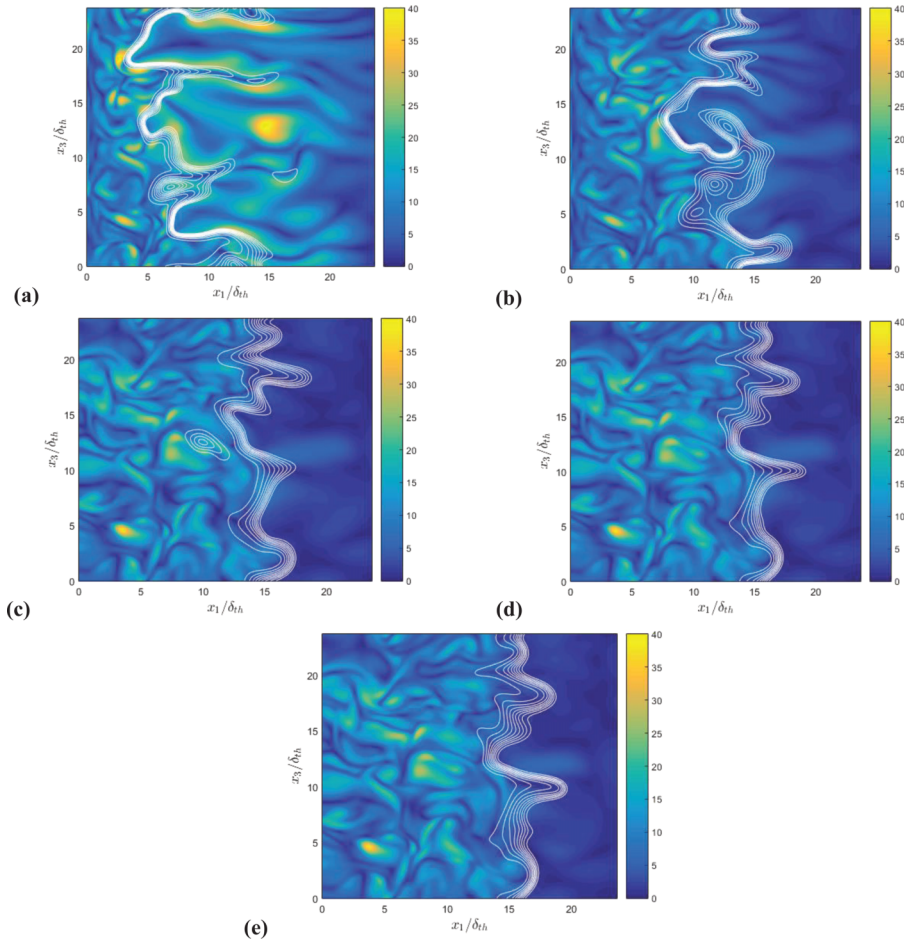


FIG. 1. Distribution of $(\omega_i \omega_i)^{\frac{1}{2}} \times \delta_{th} / S_L$ in the central $x_1 - x_3$ plane at time $t = t_{chem}$ for the $Le =$ (a) 0.34, (b) 0.6, (c) 0.8, (d) 1.0, and (e) 1.2 cases.

respectively). Table I also lists the normalised values of the volume-integrated reaction rate of progress variable R_T/R_L (where $R = \int_V \dot{\omega} dV$), which show that R_T/R_L increases significantly with decreasing Le . The increases in A_T/A_L and R_T/R_L with decreasing Le are caused by faster (slower) diffusion of reactants (heat) into (from) reaction zones which are positively stretched by turbulent eddies. This physical mechanism leads to a local increase in burning rate, accelerates the self-propagation of such zones, and increases their resistance to quenching due to high stretch rates, thus allowing these zones to advance far into unburned gas. On the contrary, if $Le > 1$, thermal diffusion from the stretched reaction zones dominates over reactant diffusion into these zones, thus reducing the local rate of burning and flame wrinkling, particularly when compared to the corresponding turbulent $Le = 1.0$ flame.

TABLE I. The effects of Lewis number on normalised volume-integrated reaction rate of progress variable R_T/R_L and normalised flame surface area A_T/A_L after 3.34 initial eddy turn over times.

Le	R_T/R_L	A_T/A_L
0.34	13.70	3.93
0.6	4.58	2.66
0.8	2.53	2.11
1.0	1.83	1.84
1.2	1.50	1.76

Local increases in burning rate and self-acceleration of upstream-pointing bulges in turbulent flames with $Le < 1$ are qualitatively similar to those in the corresponding laminar premixed flames due to the imbalances between the reactant and heat fluxes, which manifest themselves in the form of thermo-diffusive instability with respect to weak perturbations. This instability was investigated in a number of previous analyses.^{30,55,68–72} The linear stability analysis of thermo-diffusive instability for planar^{33–36} and spherical^{73,74} laminar premixed flames resulted in analytical expressions for the instability growth rate and largest wavenumber (smallest wavelength) of a perturbation that could trigger the instability. Interested readers are referred to Refs. 75–79 and the reviews conducted in Refs. 70–72 for the latest developments in the linear stability analysis of laminar premixed flames with $Le < 1$.

Several analyses^{44–53} attributed large values of A_T/A_L or R_T/R_L for turbulent premixed flames with $Le < 1$ to the thermo-diffusive instability of laminar flamelets which separate the unburned and burned gases. An alternative concept^{54,55,69,80} of the Lewis number effects in premixed turbulent combustion emphasizes the propagation of highly stretched leading reaction zones into the unburned gas (the so-called leading edge concept). However, a comparison of the thermo-diffusive instability and leading point concepts is beyond the scope of the present study.

It was previously demonstrated by Chakraborty *et al.*⁵² that the augmented rate of burning and strong flame normal acceleration for $Le \ll 1$ flames (e.g., $Le = 0.34$ flame considered here) can lead to significant flame-generated turbulence within the flame brush. For instance, Fig. 1(a) shows that the vorticity magnitude $\sqrt{\omega_i \omega_i} \times \delta_{th}/S_L$ gets significantly augmented towards the burned gas side of the flame front in the $Le = 0.34$ case. The same tendency can be discerned in some locations for the $Le = 0.6$ case, but the effects of flame generated turbulence (i.e., vorticity generation) are much weaker than for the $Le = 0.34$ flame. For the $Le \approx 1.0$ (e.g., 0.8, 1.0, and 1.2 cases) flames, the distribution of the normalised vorticity magnitude $\sqrt{\omega_i \omega_i} \times \delta_{th}/S_L$ is significantly different. It can be seen from Fig. 1 that the probability of finding large magnitudes of $\sqrt{\omega_i \omega_i} \times \delta_{th}/S_L$ decreases from the unburned to the burned gas side of the flame front for flames with $Le \approx 1.0$ (e.g., 0.8, 1.0, and 1.2 cases).

The above difference in the vorticity magnitude distribution in response to Le can further be seen from the variation of the Reynolds averaged normalised vorticity magnitude $(\omega_i \omega_i)^{1/2} \times \delta_{th}/S_L$ with Favre averaged reaction progress variable \bar{c} shown in Fig. 2(a) for the different Lewis number cases considered here. It can be seen from Fig. 2(a) that $(\omega_i \omega_i)^{1/2} \times \delta_{th}/S_L$ decays monotonically from unburned to burned gas side of the flame brush for flames with $Le \approx 1.0$ (e.g., $Le = 0.8, 1.0,$ and 1.2) cases considered here. The $Le = 0.6$ flame shows a behaviour which is qualitatively similar to the $Le \approx 1.0$ cases. However, the vorticity decay within the flame brush in the $Le = 0.6$ case is weaker than in the $Le = 0.8, 1.0,$ and 1.2 cases. A similar vorticity decay has been observed for the entropy transport for low Damköhler number (i.e., $Da < 1$) unity Lewis number combustion analysed by Hamlington *et al.*¹¹ The decay of $(\omega_i \omega_i)^{1/2} \times \delta_{th}/S_L$ across the flame brush was also observed for the corrugated flamelets regime flames by Treurniet *et al.*¹² and Lipatnikov *et al.*¹³ However, in the present simulations, the quantity $(\omega_i \omega_i)^{1/2} \times \delta_{th}/S_L$ increases from the unburned gas side to the middle of the flame brush before decaying towards the burned gas side in the $Le = 0.34$ case. A similar trend was observed in some of the high Damköhler number (i.e., $Da > 1$) unity Lewis number flames with high values of τ in previous analyses.^{12,13}

The variations of the rms values of the normalised Favre averaged vorticity $\left[\overline{\rho(\omega_i - \tilde{\omega}_i)^2 / \bar{\rho}} \right]^{1/2} \times \delta_{th}/S_L$ and its components (i.e., $\left[\overline{\rho(\omega_1 - \tilde{\omega}_1)^2 / \bar{\rho}} \right]^{1/2} \times \delta_{th}/S_L$; $\left[\overline{\rho(\omega_2 - \tilde{\omega}_2)^2 / \bar{\rho}} \right]^{1/2} \times \delta_{th}/S_L$ and $\left[\overline{\rho(\omega_3 - \tilde{\omega}_3)^2 / \bar{\rho}} \right]^{1/2} \times \delta_{th}/S_L$) with \bar{c} are shown in Figs. 2(b)–2(f) for all the different Lewis number cases considered here. Figures 2(b)–2(f) indicate that there is a difference in the magnitudes of the rms values of Favre averaged vorticity components between the direction of mean flame propagation and in the transverse directions for all cases, and this anisotropy is particularly strong in the $Le = 0.34$ case. This is consistent with previous analyses^{11–13} which revealed that the presence of the flame makes the vorticity field substantially anisotropic. It can be seen from Figs. 2(b) to

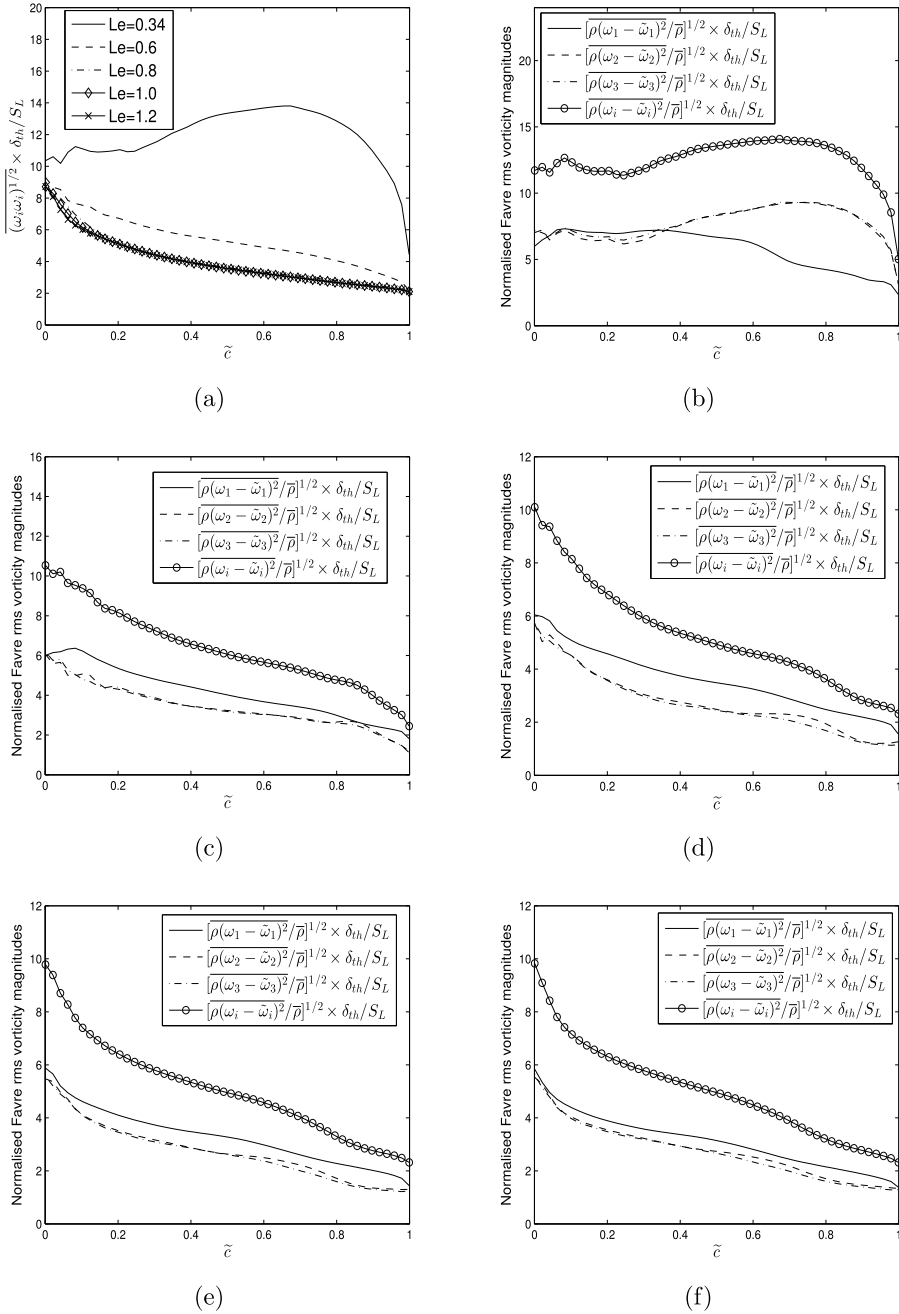


FIG. 2. (a) Variation of the Reynolds averaged normalized vorticity magnitude $\overline{(\omega_i \omega_i)^{1/2}} \times \delta_{th}/S_L$ with Favre averaged reaction progress variable \tilde{c} for all cases considered here; variations of $[\rho(\omega_i - \tilde{\omega}_i)^2/\bar{\rho}]^{1/2} \times \delta_{th}/S_L$, $[\rho(\omega_1 - \tilde{\omega}_1)^2/\bar{\rho}]^{1/2} \times \delta_{th}/S_L$, $[\rho(\omega_2 - \tilde{\omega}_2)^2/\bar{\rho}]^{1/2} \times \delta_{th}/S_L$, and $[\rho(\omega_3 - \tilde{\omega}_3)^2/\bar{\rho}]^{1/2} \times \delta_{th}/S_L$, with \tilde{c} for the flames with (b) $Le = 0.34$, (c) $Le = 0.6$, (d) $Le = 0.8$, (e) $Le = 1.0$, and (f) $Le = 1.2$.

2(f) that $[\rho(\omega_1 - \tilde{\omega}_1)^2/\bar{\rho}]^{1/2}$ monotonically decays from unburned to burned gas side of the flame brush for all cases, including the $Le = 0.34$ case. However, $[\rho(\omega_i - \tilde{\omega}_i)^2/\bar{\rho}]^{1/2}$ in the $Le = 0.34$ case shows augmentation of its magnitude from the unburned gas side to the middle of the flame brush before decreasing again towards the burned gas side of the flame brush, which is similar to the

variation of $\overline{(\omega_i \omega_i)^{1/2}}$ within the flame brush as shown in Fig. 2(a). It is evident from Fig. 2(b) that the augmentation of vorticity magnitude within the flame for the $Le = 0.34$ case originates principally due to vorticity components in the directions normal to the mean direction of flame propagation (e.g., $\left[\overline{\rho(\omega_2 - \tilde{\omega}_2)^2/\bar{\rho}}\right]^{1/2}$ and $\left[\overline{\rho(\omega_3 - \tilde{\omega}_3)^2/\bar{\rho}}\right]^{1/2}$ are responsible for the augmentation of $\left[\overline{\rho(\omega_i - \tilde{\omega}_i)^2/\bar{\rho}}\right]^{1/2}$ within the flame brush for the $Le = 0.34$ case). For other cases, all the components of rms of Favre averaged vorticity (i.e., $\left[\overline{\rho(\omega_1 - \tilde{\omega}_1)^2/\bar{\rho}}\right]^{1/2} \times \delta_{th}/S_L$; $\left[\overline{\rho(\omega_2 - \tilde{\omega}_2)^2/\bar{\rho}}\right]^{1/2} \times \delta_{th}/S_L$ and $\left[\overline{\rho(\omega_3 - \tilde{\omega}_3)^2/\bar{\rho}}\right]^{1/2} \times \delta_{th}/S_L$ decay from the unburned to the burned gas side of the flame brush.

The variations of $\overline{(\omega_i \omega_i)^{1/2}}$, $\overline{(\omega_n \omega_n)^{1/2}}$ (here the repeated indices n do not indicate summation) and $\overline{(\omega_t \omega_t)^{1/2}}$ (here the repeated indices t indicate summation over two tangential directions) with \tilde{c} are shown in Figs. 3(a)-3(e) for the $Le = 0.34, 0.6, 0.8, 1.0,$ and 1.2 cases, respectively, where $\omega_n \omega_n = N_i N_j \omega_i \omega_j$ and $\omega_t \omega_t = (\delta_{ij} - N_i N_j) \omega_i \omega_j$ are the flame normal and flame tangential vorticity components, respectively, with $N_i = -(\partial c / \partial x_i) / |\nabla c|$ being the i th component of the local flame normal vector. It is evident from Figs. 3(a)-3(e) that $\overline{(\omega_n \omega_n)^{1/2}}$ decays from the unburned to burned gas side of the flame for all cases. By contrast, $\overline{(\omega_t \omega_t)^{1/2}}$ decays from the unburned gas side to the middle of flame before rising again and assuming the maximum value close to the burned gas side of the flame for the $Le = 0.34$ case. The augmentation of $\overline{(\omega_t \omega_t)^{1/2}}$ within the flame is principally responsible for the generation of $\overline{(\omega_i \omega_i)^{1/2}}$ within the flame for the $Le = 0.34$ case. The quantity $\overline{(\omega_t \omega_t)^{1/2}}$ decays from the unburned to the burned gas side of the flame for the $Le = 0.6, 0.8, 1.0$ and 1.2 cases considered here. Assuming two tangential directions are statistically similar, the variations of $\overline{(\omega_t \omega_t / 2)^{1/2}}$ are also compared with the distributions of $\overline{(\omega_n \omega_n)^{1/2}}$ in Figs. 3(a)-3(e). It can be seen from Figs. 3(a)-3(e) that there are significant differences in the distributions of $\overline{(\omega_t \omega_t / 2)^{1/2}}$ and $\overline{(\omega_n \omega_n)^{1/2}}$ within the flame brush for all cases but the degree of anisotropy between $\overline{(\omega_t \omega_t / 2)^{1/2}}$ and $\overline{(\omega_n \omega_n)^{1/2}}$ increases with decreasing Le . The anisotropic behaviour of vorticity components in Figs. 3(a)-3(e) is consistent with the behaviour of Favre mean vorticity components shown in Figs. 2(b)-2(f), respectively. The flame normal direction for statistically planar flames predominantly coincides with the mean direction of flame propagation (i.e., x_1 -direction), and thus the variation of $\overline{(\omega_n \omega_n)^{1/2}}$ ($\overline{(\omega_t \omega_t / 2)^{1/2}}$) has been found to be qualitatively similar to $\left[\overline{\rho(\omega_1 - \tilde{\omega}_1)^2/\bar{\rho}}\right]^{1/2}$ ($\left[\overline{\rho(\omega_2 - \tilde{\omega}_2)^2/\bar{\rho}}\right]^{1/2}$ and $\left[\overline{\rho(\omega_3 - \tilde{\omega}_3)^2/\bar{\rho}}\right]^{1/2}$). Furthermore, a comparison between Figs. 1-3 reveals that the decay of vorticity magnitude from the unburned to the burned gas side weakens with decreasing global Lewis number Le even though flames are subjected to statistically similar turbulent flow field on the unburned gas side of the flame.

It is instructive to investigate the statistical behaviour of the terms of the vorticity and enstrophy transport equations (i.e., Eqs. (2) and (3)) in order to understand the influences of global Lewis number Le on the vorticity and enstrophy transports. The variations of the normalised values of $\overline{(t_{1t} t_{1t})^{1/2}}$, $\overline{(t_{21t} t_{21t})^{1/2}}$, $\overline{(t_{22t} t_{22t})^{1/2}}$, $\overline{(t_{3t} t_{3t})^{1/2}}$, and $\overline{(t_{4t} t_{4t})^{1/2}}$ with \tilde{c} are shown in Figs. 4(a)-4(e) for the $Le = 0.34, 0.6, 0.8, 1.0,$ and 1.2 cases, respectively, where $\overline{(t_{qt} t_{qt})^{1/2}} = \overline{[(\delta_{ij} - N_i N_j) t_{qi} t_{qj}]^{1/2}} = \left(\vec{t}_q \cdot \vec{t}_q - (t_q \cdot \vec{N})^2\right)^{1/2}$ with $q = 1, 21, 22, 3,$ and 4 . The corresponding variations of the normalised values of $\overline{(t_{1n} t_{1n})^{1/2}}$, $\overline{(t_{21n} t_{21n})^{1/2}}$, $\overline{(t_{22n} t_{22n})^{1/2}}$, $\overline{(t_{3n} t_{3n})^{1/2}}$, and $\overline{(t_{4n} t_{4n})^{1/2}}$ with \tilde{c} are shown in Figs. 5(a)-5(e) for the $Le = 0.34, 0.6, 0.8, 1.0,$ and 1.2 cases, respectively, where $\overline{(t_{qn} t_{qn})^{1/2}} = \overline{[(N_i N_j) t_{qi} t_{qj}]^{1/2}} = \left((t_q \cdot \vec{N})^2\right)^{1/2}$ with $q = 1, 21, 22, 3,$ and 4 . The quantities $\overline{(t_{qn} t_{qn})^{1/2}}$ and $\overline{(t_{qt} t_{qt})^{1/2}}$ could be interpreted as the Reynolds averaged values of the magnitudes of the components of the vector \vec{t}_q (where $q = 1, 21, 22, 3,$ and 4) in local flame normal and tangential directions, as used in a previous analysis.¹³ It is worth noting that $\overline{(t_{qn} t_{qn})^{1/2}}$ and $\overline{(t_{qt} t_{qt})^{1/2}}$ are not the Reynolds averaged magnitudes of the terms of the transport equation of $\overline{\omega_n} = N_i \omega_j N_j$ and $\overline{\omega_t} = (\omega_i - \omega_j N_i N_j)$,

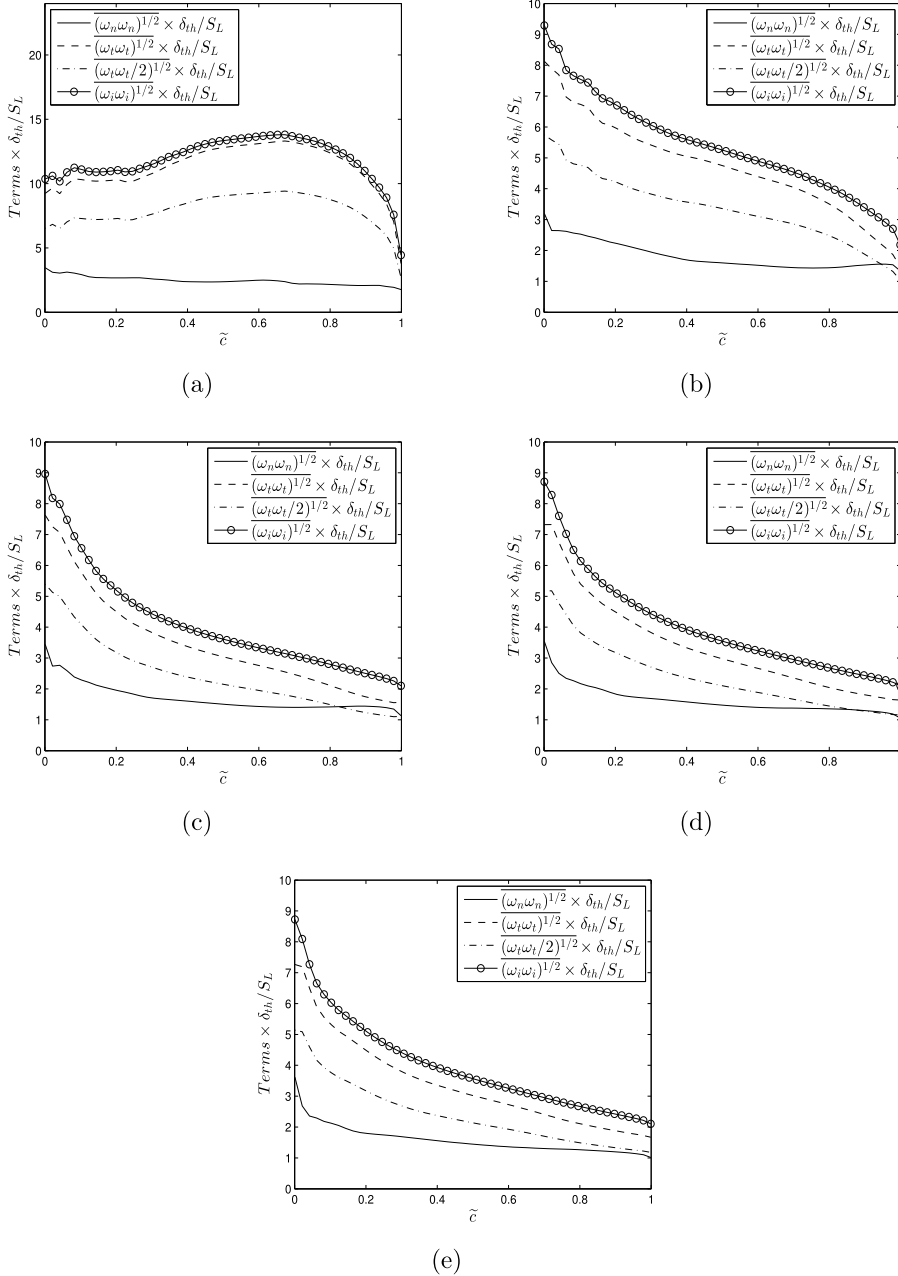


FIG. 3. Variation of $\overline{(\omega_i\omega_i)^{1/2}} \times \delta_{th}/S_L$, $\overline{(\omega_n\omega_n)^{1/2}} \times \delta_{th}/S_L$, $\overline{(\omega_t\omega_t)^{1/2}} \times \delta_{th}/S_L$, and $\overline{(\omega_t\omega_t/2)^{1/2}} \times \delta_{th}/S_L$ with Favre averaged reaction progress variable \tilde{c} for the $Le =$ (a) 0.34, (b) 0.6, (c) 0.8, (d) 1.0, and (e) 1.2 cases.

respectively, under general conditions. Instead, $\overline{(t_{qt}t_{qn})^{1/2}}$ and $\overline{(t_{qt}t_{qt})^{1/2}}$ are associated with terms of the transport equation of $\overline{N_iN_jD\omega_j/Dt}$ and $\overline{(\delta_{ij} - N_iN_j)D\omega_j/Dt}$, respectively. Interested readers are referred to [Appendix B](#) for further discussion in this regard. The quantities $\overline{(t_{qt}t_{qt})^{1/2}}$ and $\overline{(t_{qn}t_{qn})^{1/2}}$ can only be interpreted as the terms of the transport equation of $\overline{\omega_t} = (\omega_i - \omega_jN_iN_j)$ and $\overline{\omega_n} = \overline{N_i\omega_jN_j}$ under the strong assumption that the rotation of the moving frame of reference is ignored, which amounts to $\overline{\omega_jD(N_iN_j)/Dt} = 0$. Nevertheless, the difference between $\overline{D\omega_n/Dt} = \overline{D(N_iN_j\omega_j)/Dt}$ and $\overline{N_iN_jD\omega_j/Dt}$, or between $\overline{D\omega_i/Dt}$ and $\overline{[D\omega_i/dt - N_iN_jD\omega_j/Dt]}$, is sufficiently small in comparison to the magnitudes of $\overline{(t_{qn}t_{qn})^{1/2}}$ or $\overline{(t_{qt}t_{qt})^{1/2}}$ under the conditions of the present DNS (see Fig. 11

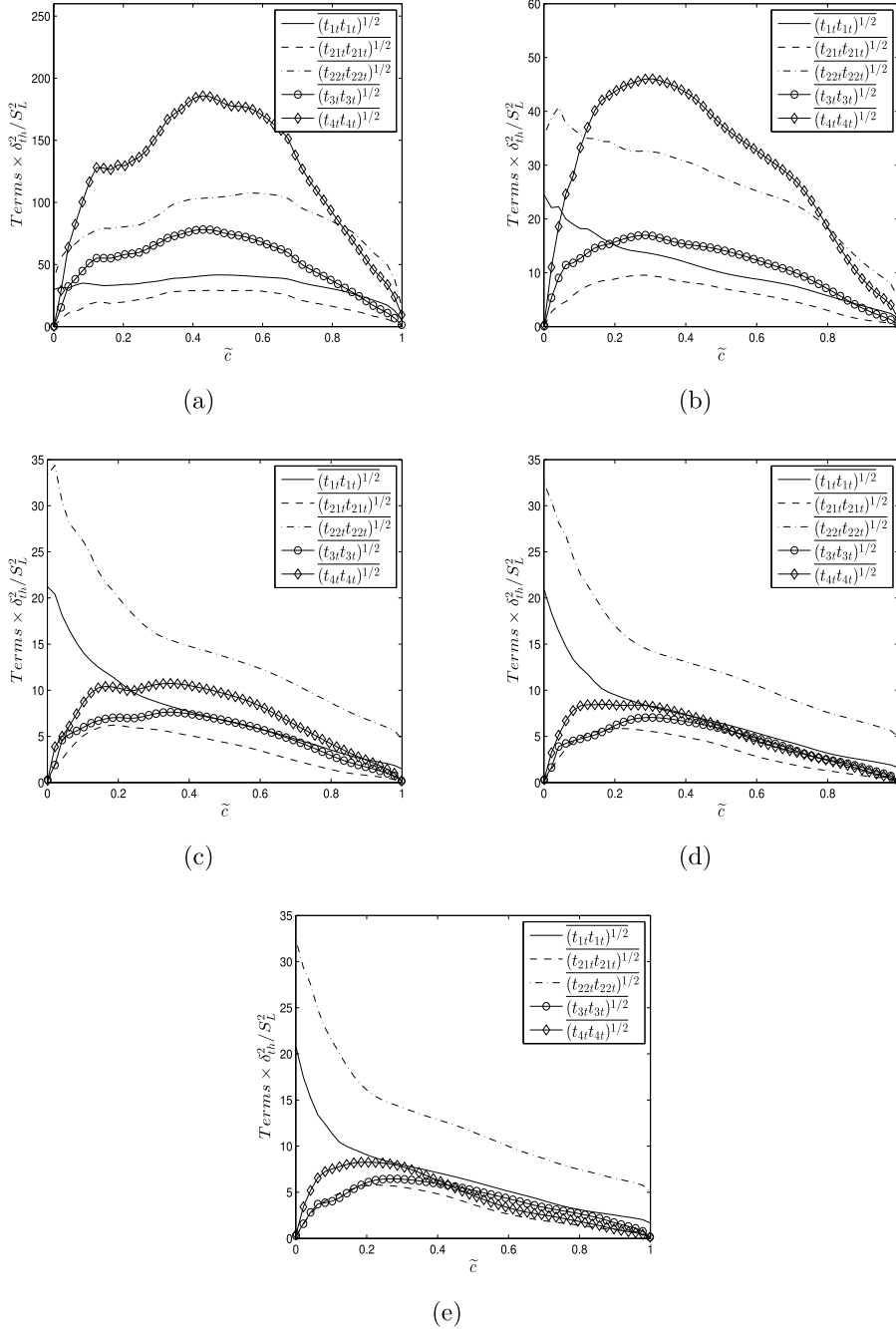


FIG. 4. Variations of $\overline{(t_{1t}t_{1t})}^{1/2} \times \delta_{th}^2 / S_L^2$, $\overline{(t_{21t}t_{21t})}^{1/2} \times \delta_{th}^2 / S_L^2$, $\overline{(t_{22t}t_{22t})}^{1/2} \times \delta_{th}^2 / S_L^2$, $\overline{(t_{3t}t_{3t})}^{1/2} \times \delta_{th}^2 / S_L^2$, and $\overline{(t_{4t}t_{4t})}^{1/2} \times \delta_{th}^2 / S_L^2$ with \tilde{z} for the $Le =$ (a) 0.34, (b) 0.6, (c) 0.8, (d) 1.0, and (e) 1.2 cases.

in Appendix B). Accordingly, $\overline{(t_{qn}t_{qn})}^{1/2}$ and $\overline{(t_{qt}t_{qt})}^{1/2}$ represent magnitudes of the leading order contributors to the transport equation of $\overline{\omega_n} = N_i \omega_j N_j$ and $\overline{\omega_t} = (\omega_i - \omega_j N_i N_j)$, respectively.

A comparison between Figs. 4 and 5 reveals that the magnitude of the baroclinic torque contribution $\overline{(t_{4t}t_{4t})}^{1/2}$ remains much greater than the magnitude of $\overline{(t_{4n}t_{4n})}^{1/2}$ in the $Le = 0.34$ case. Nevertheless, the latter quantity does not vanish in the low Le flames, because vectors $\nabla \rho$ and ∇c are not exactly parallel in this case, contrary to an adiabatic flame with $Le = 1.0$, where $\nabla \rho$ and ∇c are exactly parallel, and, hence, the normal component of $\nabla \rho \times \nabla p$ and the baroclinic term $\overline{(t_{4n}t_{4n})}^{1/2}$

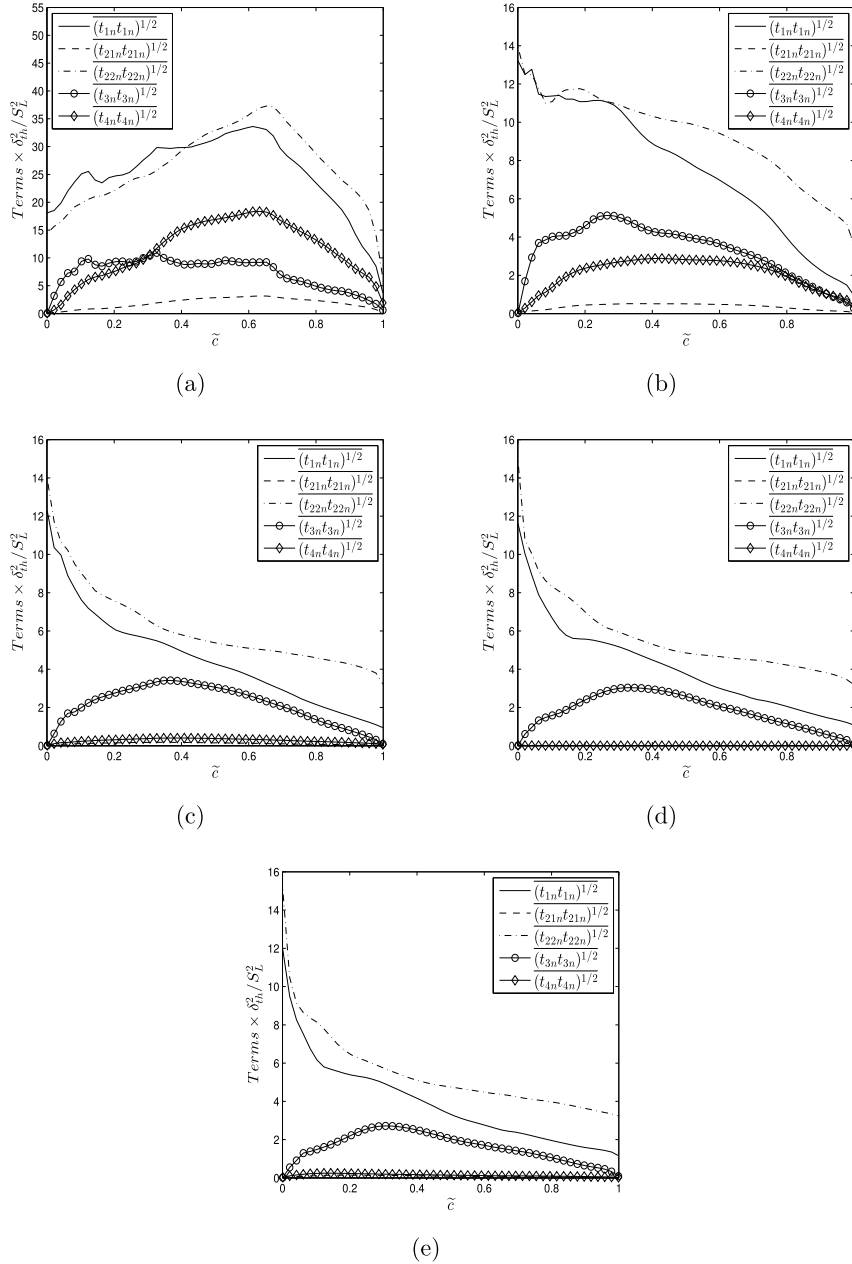


FIG. 5. Variations of $\overline{(t_{1n}t_{1n})}^{1/2} \times \delta_{th}^2/S_L^2$, $\overline{(t_{21n}t_{21n})}^{1/2} \times \delta_{th}^2/S_L^2$, $\overline{(t_{22n}t_{22n})}^{1/2} \times \delta_{th}^2/S_L^2$, $\overline{(t_{3n}t_{3n})}^{1/2} \times \delta_{th}^2/S_L^2$, and $\overline{(t_{4n}t_{4n})}^{1/2} \times \delta_{th}^2/S_L^2$ with \tilde{c} for the $Le =$ (a) 0.34, (b) 0.6, (c) 0.8, (d) 1.0, and (e) 1.2 cases.

vanish. This behaviour can be explained in the following manner. The mixture density ρ can be expressed as $\rho = \rho_0/(1 + \tau T)$ for flames with constant molecular weight (as in the present DNS), where $T = (\hat{T} - T_0)/(T_{ad} - T_0)$ is the non-dimensional temperature.⁸¹ The non-dimensional temperature T can be equated to c for globally adiabatic, low Mach number $Le = 1.0$ flames, which leads to $\nabla \rho = -\tau \rho^2 \nabla c / \rho_0 = \tau \rho^2 |\nabla c| \vec{N} / \rho_0$. Thus, the vectors $\nabla \rho$ and ∇c are parallel (alternatively $\nabla \rho \times \nabla p$ and $\vec{N} = -\nabla c / |\nabla c|$ are mutually perpendicular) in the $Le = 1.0$ flame considered here. It is worth noting that $c \neq T$ for non-unity Lewis number flames and the quantities increasingly deviate from each other with decreasing Le . As a result, $\nabla \rho = -\tau \rho^2 \nabla T / \rho_0 \neq \tau \rho^2 |\nabla c| \vec{N} / \rho_0$ for flames with $Le \neq 1.0$ and thus $\nabla \rho \times \nabla p$ and $\vec{N} = -\nabla c / |\nabla c|$ are not mutually perpendicular to each other. This gives rise to non-zero values of $\overline{(t_{4n}t_{4n})}^{1/2}$ in the non-unity Lewis number flames.

It is evident from Fig. 4 that the baroclinic torque contribution (i.e., $\overline{(t_{4t}t_{4t})^{1/2}}$) dominates over the magnitudes of other contributions (i.e., $\overline{(t_{1t}t_{1t})^{1/2}}$, $\overline{(t_{21t}t_{21t})^{1/2}}$, $\overline{(t_{22t}t_{22t})^{1/2}}$, and $\overline{(t_{3t}t_{3t})^{1/2}}$) for the $Le = 0.34$ and 0.6 cases, whereas the magnitude of $\overline{(t_{4n}t_{4n})^{1/2}}$ remains smaller than the magnitudes of $\overline{(t_{1n}t_{1n})^{1/2}}$, $\overline{(t_{22n}t_{22n})^{1/2}}$, and $\overline{(t_{3n}t_{3n})^{1/2}}$ and comparable to $\overline{(t_{21n}t_{21n})^{1/2}}$. Thus the baroclinic term t_4 is principally responsible for the anisotropy of the vorticity components within the flame brush in the $Le = 0.34$ and 0.6 cases. For $Le \approx 1.0$ cases, the contribution of baroclinic torque $\overline{(t_{4t}t_{4t})^{1/2}}$ remains comparable to $\overline{(t_{1t}t_{1t})^{1/2}}$, $\overline{(t_{21t}t_{21t})^{1/2}}$, $\overline{(t_{22t}t_{22t})^{1/2}}$, and $\overline{(t_{3t}t_{3t})^{1/2}}$, whereas the baroclinic term $\overline{(t_{4n}t_{4n})^{1/2}}$ remains negligible in comparison to $\overline{(t_{1n}t_{1n})^{1/2}}$, $\overline{(t_{22n}t_{22n})^{1/2}}$, and $\overline{(t_{3n}t_{3n})^{1/2}}$.

Under conditions of the present DNS, the viscous diffusion term t_{22} plays an important role in the Reynolds averaged vorticity transport (see Eq. (2)). For instance, the viscous diffusion term $\overline{(t_{22t}t_{22t})^{1/2}}$ is significantly greater than the vortex stretching term $\overline{(t_{1t}t_{1t})^{1/2}}$ in all five cases, see Fig. 4, while the magnitudes of the normal components of these two terms (i.e., $\overline{(t_{1n}t_{1n})^{1/2}}$ and $\overline{(t_{22n}t_{22n})^{1/2}}$) are comparable in the major part of the flame brush in each case, see Fig. 5. These observations are associated with relatively moderate values of turbulent Reynolds number Re_t for the cases considered here, whereas the vortex stretching term is expected to dominate at high values of Re_t . It can be seen from Fig. 3 that a strong augmentation of the vorticity magnitude in the transverse direction takes place within the flame brush, which also sets up a strong vorticity gradient within the flame in the $Le = 0.34$ case. This gives rise to an increase in the magnitudes of the vortex-stretching (i.e., $\omega_j(\partial u_i/\partial x_j)$) and the dissipation (i.e., $-\nu(\partial \omega_i/\partial x_j)(\partial \omega_i/\partial x_j)$) contributions to the components of vorticity transport terms in flame tangential direction, and thus $\overline{(t_{1t}t_{1t})^{1/2}}$ and $\overline{(t_{22t}t_{22t})^{1/2}}$ rise from the unburned gas side and assume peak values within the flame brush before decreasing again on the burned gas side for the $Le = 0.34$ case. The vorticity magnitude in the transverse direction decreases monotonically from the unburned to the burned gas side of the flame brush for the other cases, and thus $\overline{(t_{1t}t_{1t})^{1/2}}$ and $\overline{(t_{22t}t_{22t})^{1/2}}$ decrease monotonically from the unburned to the burned gas side of the flame brush for the other (i.e., $Le = 0.6, 0.8, 1.0$, and 1.2) cases.

It can be seen from Figs. 4 and 5 that the contributions of dilatation and baroclinic torque in both flame normal and tangential directions (i.e., $\overline{(t_{3n}t_{3n})^{1/2}}$, $\overline{(t_{4n}t_{4n})^{1/2}}$, $\overline{(t_{3t}t_{3t})^{1/2}}$, and $\overline{(t_{4t}t_{4t})^{1/2}}$) vanish both in the unburned and burned gas sides of the flame brush as the effects of density variation and dilatation rate diminish both in the unburned and burned gas sides of the flame brush. Furthermore, Figs. 4 and 5 indicate that the relative contributions of viscous torque due to density variation, dilatation, and baroclinic terms (i.e., t_{21} , t_3 , and t_4) weaken, and their magnitudes decrease, with increasing Le . The vorticity transport for the $Le \approx 1.0$ (i.e., $Le = 0.8, 1.0$, and 1.2) cases considered here is principally determined by the vortex stretching and viscous diffusion (i.e., t_1 and t_{22} in Eq. (2)), which is similar to the vorticity transport for non-reacting flows.

It is evident from Eq. (2) that the dilatation contribution destroys all vorticity components irrespective of the direction due to predominantly positive dilatation rate $\partial u_i/\partial x_i$ values in premixed flames. The rate of burning diminishes with increasing Le , which is reflected in the decrease in the mean value of normalised dilatation rate $(\partial u_i/\partial x_i) \times \delta_{th}/S_L$ magnitude with increasing Le , as shown in Fig. 6(a). This increase in the magnitude of dilatation rate $\partial u_i/\partial x_i$ for small values of Lewis number is responsible for increased magnitudes of $t_3 = -(\partial u_k/\partial x_k)\omega_i$ with decreasing Le . However, the magnitude of $t_{3i} = -(\partial u_k/\partial x_k)\omega_i$ does not change in proportion to $(\partial u_k/\partial x_k)$ because an increase in the dilatation term reduces the magnitude of ω_i in the term t_{3i} . It is also worth noting that $\overline{(t_{3t}t_{3t})^{1/2}}$ is comparable with $\overline{(t_{1t}t_{1t})^{1/2}}$ and $\overline{(t_{21t}t_{21t})^{1/2}}$, but is substantially smaller than $\overline{(t_{4t}t_{4t})^{1/2}}$ in the low Lewis number flames in Figs. 4(a) and 4(b). This difference between $\overline{(t_{3t}t_{3t})^{1/2}}$ and $\overline{(t_{4t}t_{4t})^{1/2}}$ is also associated with the dependence of t_{3t} on the relevant vorticity components, i.e., due to an important role played by vorticity diffusion under conditions of the present DNS, the magnitude of vorticity components is insufficient for the dilatation term to counterbalance the baroclinic torque term.

It is shown elsewhere^{48,50} that the flame thickness decreases, though the probability of finding high temperature spots (including super-adiabatic temperature values) increases with decreasing Le

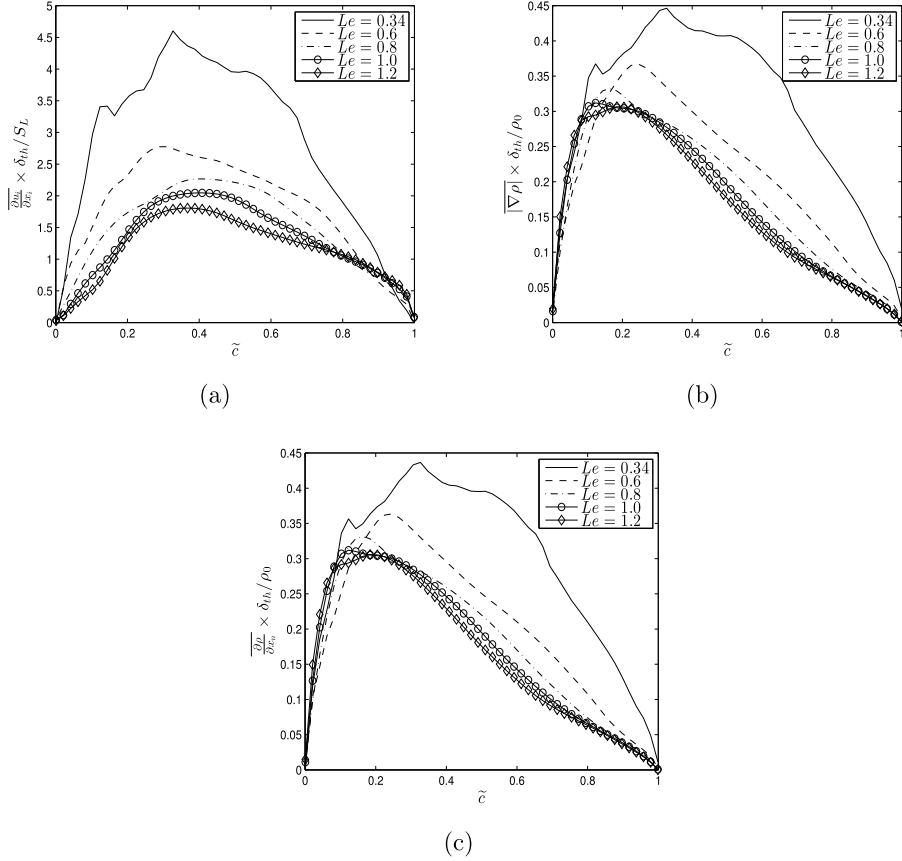


FIG. 6. Variations of (a) $\overline{(\partial u_i / \partial x_i)} \times \delta_{th} / S_L$, (b) $|\overline{\nabla \rho}| \times \delta_{th} / \rho_0$, and (c) $\overline{(\partial \rho / \partial x_n)} \times \delta_{th} / \rho_0$ with Favre averaged reaction progress variable \tilde{c} for all cases considered here.

in turbulent flames, because the molecular diffusion of reactants into the reaction zone overwhelms conductive heat flux out from the zone for small values of Le . Accordingly, the magnitude of density gradient $|\nabla \rho|$ increases with decreasing Le , which can be confirmed from Fig. 6(b) where the variation of $|\overline{\nabla \rho}| \times \delta_{th} / \rho_0$ with \tilde{c} is shown for all cases considered here. Similar effects are also observed in laminar premixed flames subject to thermo-diffusive instability.^{30,33–36,68,69}

The high magnitude of $\nabla \rho$ and the particular nature of misalignment between this vector and the divergence of the viscous stress tensor also lead to relatively large magnitudes of the effects of viscous torque due to density variation (i.e., t_{21}) in the vorticity transport equation. It can be seen from Figs. 4 and 5 that both $\overline{(t_{21t} t_{21t})}^{1/2}$ and $\overline{(t_{21n} t_{21n})}^{1/2}$ play non-negligible role in vorticity transport for small values of Le (e.g., $Le = 0.34$ case considered here). The previous analyses by Hamlington *et al.*¹¹ and Treurniet *et al.*¹² did not report any significant influences of t_{21} but Lipatnikov *et al.*¹³ reported considerable influences of t_{21} for unity Lewis number weakly turbulent flames with high values of τ , where $\nabla \rho \approx -\tau \rho^2 \nabla T / \rho_0$ is expected to assume large magnitudes.

As discussed above, for low Mach number unity Lewis number flames, the non-dimensional temperature T can be equated to c , and thus $\nabla \rho$ can be expressed as $\nabla \rho = \tau \rho^2 |\nabla c| \vec{N} / \rho_0$, which leads to $\overline{\partial \rho / \partial x_n} = \nabla \rho \cdot \vec{N} = -\tau \rho^2 \nabla T \cdot \vec{N} / \rho_0 = \tau \rho^2 |\nabla c| / \rho_0 = |\nabla \rho|$. A comparison between $|\overline{\nabla \rho}| \times \delta_{th} / \rho_0$ and $\overline{(\partial \rho / \partial x_n)} \times \delta_{th} / \rho_0$ in Fig. 6(b) reveals that these quantities are close to each other even for $Le \neq 1.0$ flames, thus, implying that $(-\nabla T \cdot \vec{N})$ remains close to $|\nabla c|$ in all simulated cases. This suggests that $\nabla \rho$ can be taken to scale as $\nabla \rho \sim \tau \rho^2 |\nabla c| \vec{N} / \rho_0$ and thus $\nabla \rho$ mostly aligns with the flame normal direction. This suggests that the baroclinic torque $\rho^{-2} \nabla \rho \times \nabla p$ is expected to have weak contributions in the flame normal direction but its contribution to vorticity transport in tangential directions is likely to be strong, as indicated by Figs. 4 and 5.

The variations of $|\overline{(\nabla p)_t}|$, $|\overline{(\nabla p)_n}|$, and $|\overline{\nabla p}|$ are reported in Figs. 7(a)-7(e) for $Le = 0.34, 0.6, 0.8, 1.0$, and 1.2 cases, respectively. Figures 7(a)-7(e) show that $|\overline{(\nabla p)_t}|$ and $|\overline{(\nabla p)_n}|$ remain comparable, where $|\overline{(\nabla p)_n}| = |\vec{N} \cdot \nabla p|$ is associated with locally normal flow acceleration, and the pressure gradient in tangential direction at a given location is induced by heat release in the surrounding flame wrinkles and by turbulent eddies.

For a planar laminar flame surface, one obtains $N_1 = -1$, $N_2 = 0$, and thus one obtains $|\vec{N} \cdot \vec{e}_1| = 1.0$. The extent of flame wrinkling within the flame brush can be quantified with the help of the

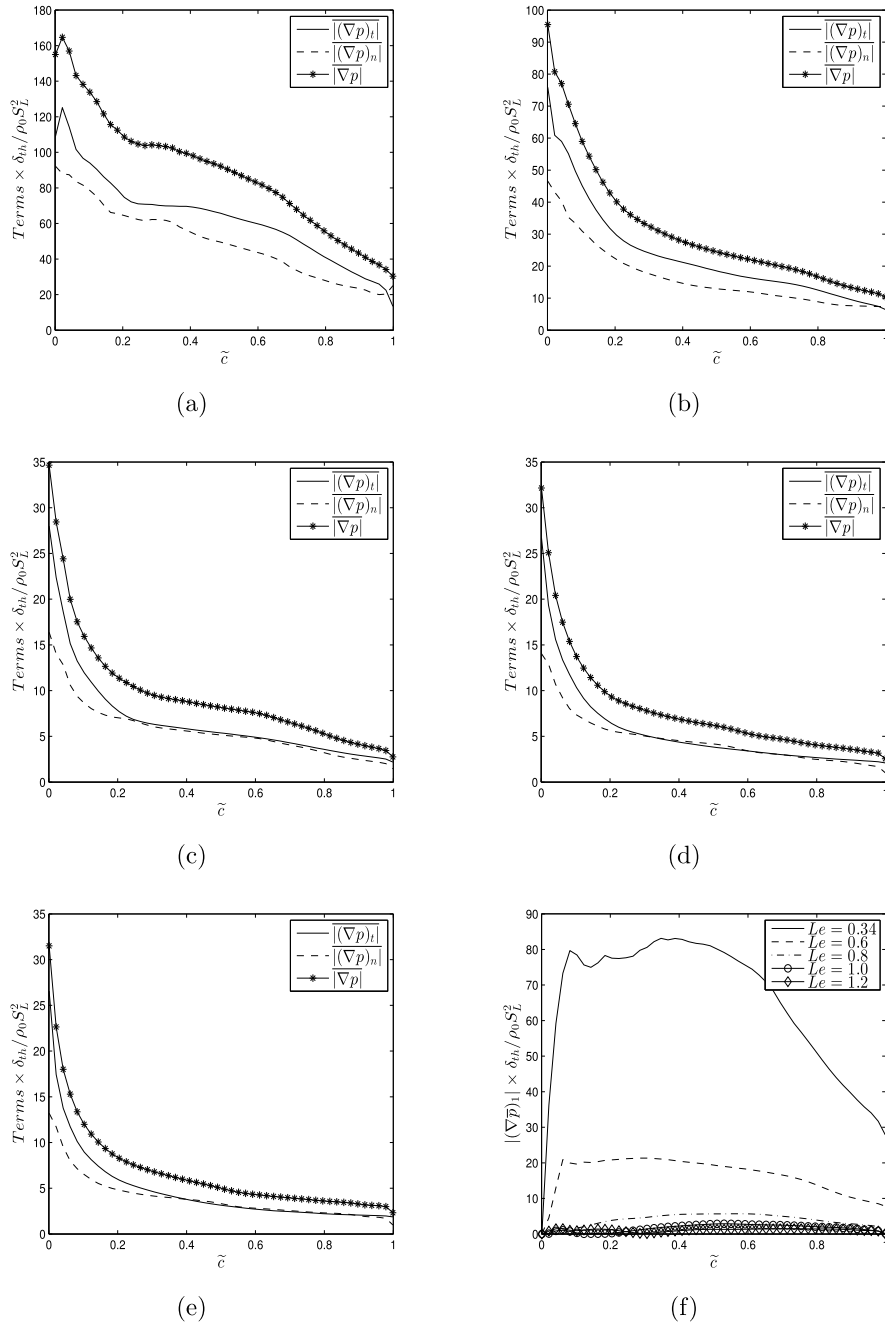


FIG. 7. Variations of $|\overline{(\nabla p)_t}| \times \delta_{th} / \rho_0 S_L^2$, $|\overline{(\nabla p)_n}| \times \delta_{th} / \rho_0 S_L^2$, and $|\overline{\nabla p}| \times \delta_{th} / \rho_0 S_L^2$ with Favre averaged reaction progress variable \tilde{c} for the $Le =$ (a) 0.34, (b) 0.6, (c) 0.8, (d) 1.0, and (e) 1.2 cases. (f) Variations of $|\overline{(\nabla \bar{p})}_1| \times \delta_{th} / \rho_0 S_L^2$ with Favre averaged reaction progress variable \tilde{c} for all cases considered here.

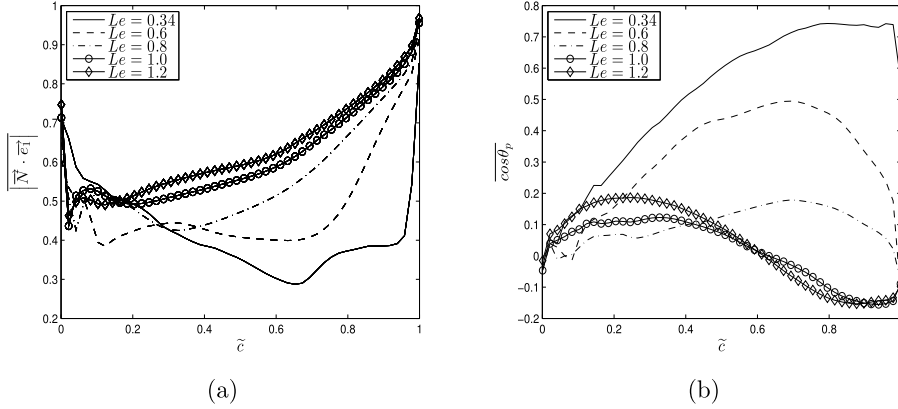


FIG. 8. Variations of (a) $|\vec{N} \cdot \vec{e}_1|$ and (b) $\overline{\cos \theta_p} = \overline{(\nabla \rho \times \nabla p) \cdot \vec{\omega}} / (|\nabla \rho \times \nabla p| \cdot |\vec{\omega}|)$ with Favre averaged reaction progress variable \tilde{c} for all cases considered here.

departure of $|\vec{N} \cdot \vec{e}_1|$ from 1.0, where \vec{e} is the unit vector in the direction of mean flame propagation. The variations of $|\vec{N} \cdot \vec{e}_1|$ with \tilde{c} for all cases are shown in Fig. 8(a). It can be seen from Figs. 7 and 8(a) that the cases with small values of $|\vec{N} \cdot \vec{e}_1|$ exhibit relatively large magnitudes of $|\overline{(\nabla p)_t}|$. For example, a low magnitude of $|\vec{N} \cdot \vec{e}_1|$ and a high magnitude of $|\overline{(\nabla p)_t}|$ are obtained in the $Le = 0.34$ case, because the flame surface is more wrinkled and thus the probability of its alignment with \vec{e}_1 is likely to be small, as can be inferred from Fig. 1(a).

Moreover, an increase in turbulent burning rate due to a decrease in Le (see Table I) results in an increasing magnitude of mean pressure gradient $|(\nabla \bar{p})_1|$ normal to the mean flame brush, which can be substantiated from Fig. 7(f). This effect also contributes to the aforementioned increase in $|\overline{(\nabla p)_t}|$ with decreasing Le , because the probability of finding a substantial angle between $(\nabla \bar{p})_1$ and \vec{N} is sufficiently large in the $Le = 0.34$ case. As a result, the magnitude of $\rho^{-2} \nabla \rho \times \nabla p$ is high in this case. As the extent of flame wrinkling and the magnitude of $|(\nabla \bar{p})_1|$ diminish with increasing Le , the mean magnitude of the tangential pressure gradient and relative contribution of baroclinic torque weakens with an increase in Lewis number. Interested readers are referred to Ref. 51 for further discussion on the effects of Le on $|(\nabla \bar{p})_1|$, which is not repeated here for the sake of conciseness.

It is worth noting that baroclinic torque not only generates vorticity but also damps vorticity, depending of an angle between the vectors $\vec{\omega}$ and $\rho^{-2} \nabla \rho \times \nabla p$. This angle is characterized by $\cos \theta_p = (\nabla \rho \times \nabla p) \cdot \vec{\omega} / (|\nabla \rho \times \nabla p| \cdot |\vec{\omega}|)$. The variation of $\cos \theta_p$ with \tilde{c} for all cases considered here are shown in Fig. 8(b). It can be seen that the directions of $\vec{\omega}$ and $\rho^{-2} \nabla \rho \times \nabla p$ are completely independent of each other for leading and trailing edges of the flame brush for the $Le = 0.6, 0.8, 1.0,$ and 1.2 flames. However, in the $Le = 0.34$ flame, the directions of $\vec{\omega}$ and $\rho^{-2} \nabla \rho \times \nabla p$ are related on the burned gas side due to significant density variation caused by temperature inhomogeneity in the burned gas. Within the flame brush, $\cos \theta_p$ assumes relatively high magnitudes and this effect is particularly strong for the $Le = 0.34$ case where the tangential components of $\rho^{-2} \nabla \rho \times \nabla p$ are principally responsible for the augmentation of $(\omega_t \omega_t)^{1/2}$ within the flame brush.

The variations of the normalised values of the terms of the right hand side of the enstrophy transport equation (i.e., $T_I, T_{II}, T_{III}, T_{IV}$ and T_V) with \tilde{c} are shown in Figs. 9(a)-9(e) for $Le = 0.34, 0.6, 0.8, 1.0,$ and 1.2 cases, respectively. It can be seen that the mean contribution of vortex-stretching term T_I remains positive throughout the flame brush for all cases. The vortex-stretching term T_I can be expressed as

$$T_I = \overline{2\Omega(e_\alpha \cos^2 \alpha + e_\beta \cos^2 \beta + e_\gamma \cos^2 \gamma)}, \quad (5)$$

where $e_\alpha, e_\beta,$ and e_γ are the most extensive, compressive, and the most compressive principal strain rates, and $\alpha, \beta,$ and γ are the angles between $\vec{\omega}$ and the principal strain rate directions associated with $e_\alpha, e_\beta,$ and $e_\gamma,$ respectively. It was previously shown by Chakraborty¹⁸ that Le significantly affects

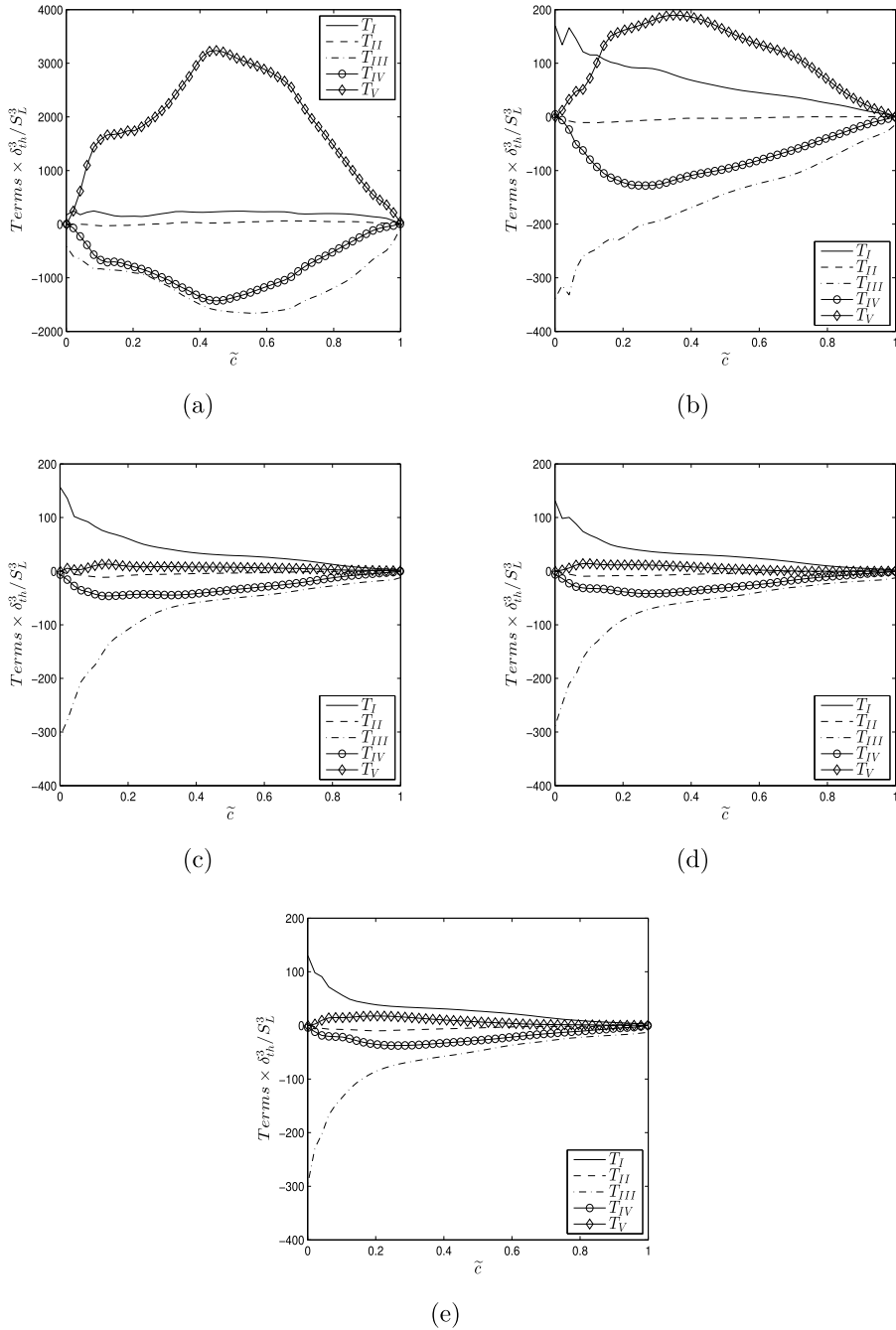


FIG. 9. Variations of $T_I \times \delta_{th}^3 / S_L^3$, $T_{II} \times \delta_{th}^3 / S_L^3$, $T_{III} \times \delta_{th}^3 / S_L^3$, $T_{IV} \times \delta_{th}^3 / S_L^3$, and $T_V \times \delta_{th}^3 / S_L^3$ with \tilde{z} for the $Le =$ (a) 0.34, (b) 0.6, (c) 0.8, (d) 1.0, and (e) 1.2 cases.

the alignment of $\vec{\omega}$ with the most extensive and compressive principal strain rates and the extent of alignment with the most extensive strain rate decreases with decreasing Le but the vortex-stretching term T_I acts to generate enstrophy for all Le cases irrespective of the nature of the alignment between $\vec{\omega}$ and the principal strain rates. Interested readers are referred to Ref. 18 for further information in this regard. The correlation between density variation and viscous action T_{II} remains small in magnitude in comparison to the other terms. The viscous dissipation term T_{III} acts as a major sink term for all cases. It is worth remembering that T_{III} includes the contributions from the viscous diffusion and dissipation of enstrophy, with the latter contribution being always negative. Under conditions of the

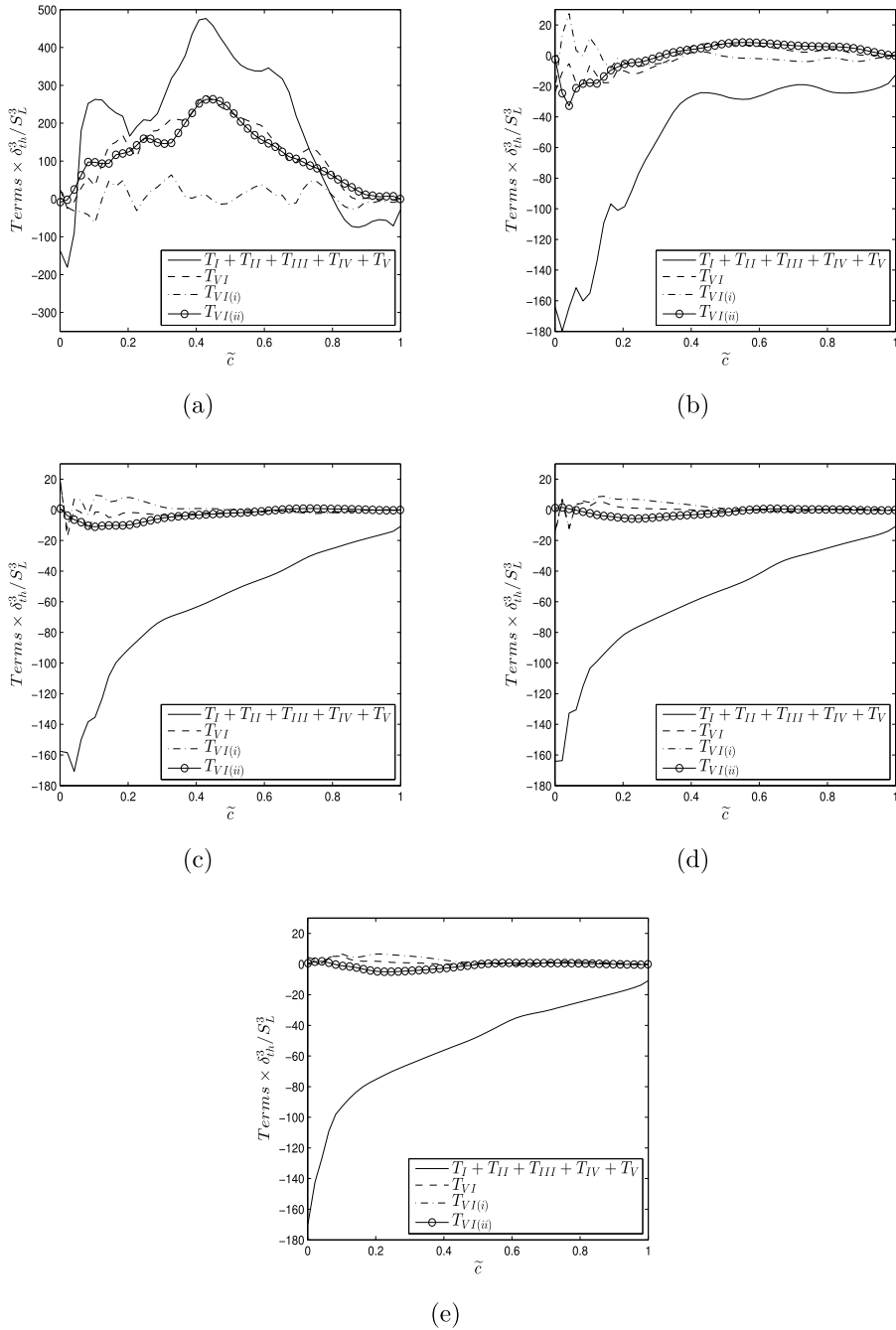


FIG. 10. Variations of $(T_I + T_{II} + T_{III} + T_{IV} + T_V) \times \delta_{th}^3/S_L^3$, $T_{VI} \times \delta_{th}^3/S_L^3$, $T_{VI(i)} \times \delta_{th}^3/S_L^3$, and $T_{VI(ii)} \times \delta_{th}^3/S_L^3$ with \tilde{z} for the $Le =$ (a) 0.34, (b) 0.6, (c) 0.8, (d) 1.0, and (e) 1.2 cases.

present DNS, the magnitudes of the viscous diffusion and dissipation of enstrophy are comparable, but the latter mechanism is expected to dominate at high Reynolds numbers. The dilatation rate term T_{IV} assumes non-zero negative values only within the flame brush. However, the magnitude of the dilatation rate term T_{IV} remains small in comparison to the viscous dissipation term T_{III} for the $Le \approx 1.0$ cases considered here but the magnitude of T_{IV} becomes comparable to T_{III} for the low Le flames (e.g., $Le = 0.34$ and 0.6 cases considered here). The baroclinic torque term T_V generates enstrophy within the flame brush but vanishes both in the unburned and burned gas sides.

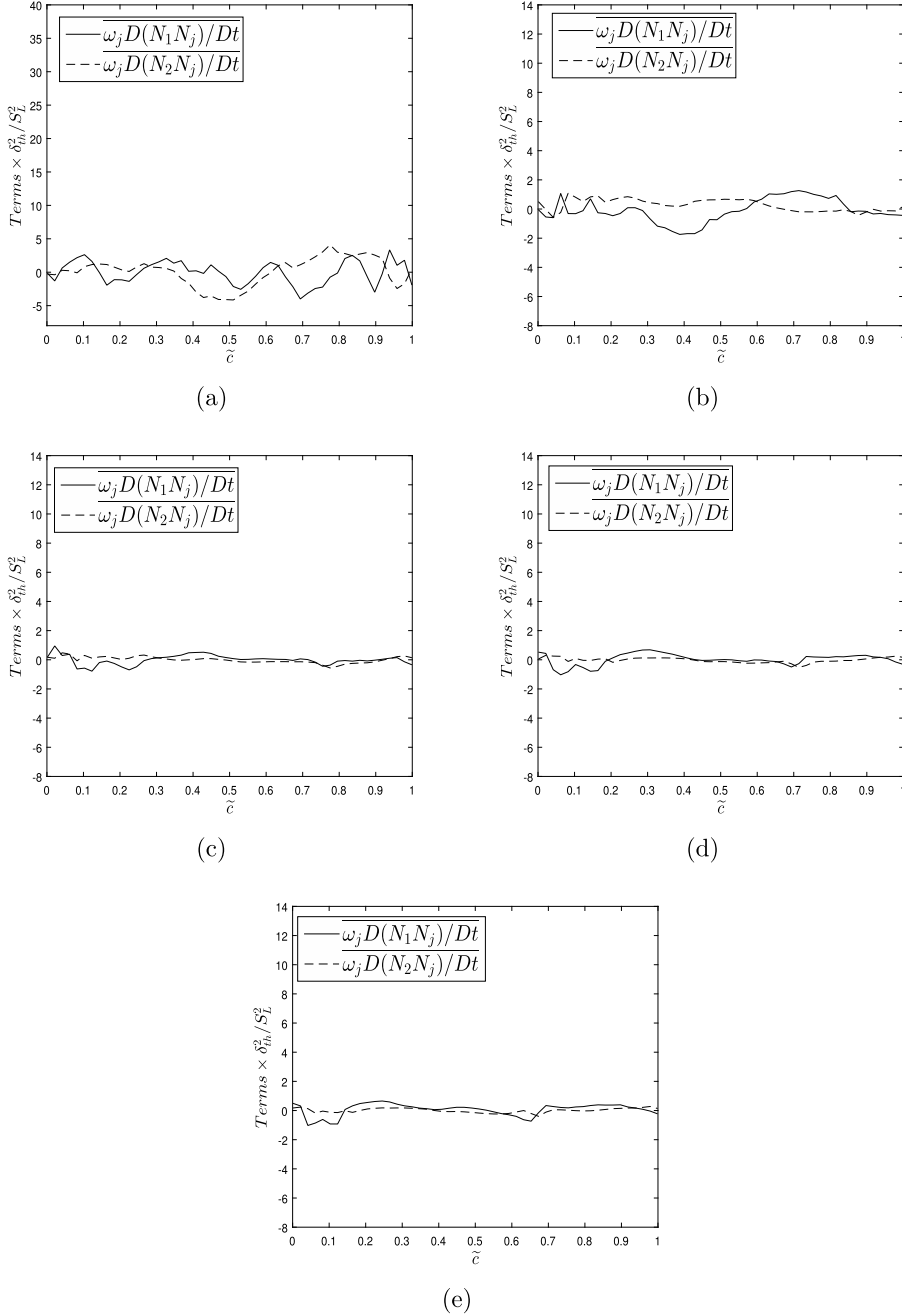


FIG. 11. Variations of $\overline{\omega_j D(N_1 N_j)/Dt} \times \delta_m^2/S_L^2$ and $\overline{\omega_j D(N_2 N_j)/Dt} \times \delta_m^2/S_L^2$ with \tilde{c} for cases with $Le =$ (a) 0.34, (b) 0.6, (c) 0.8, (d) 1.0, and (e) 1.2. The variation of $\overline{\omega_j D(N_3 N_j)/Dt} \times \delta_m^2/S_L^2$ is not explicitly shown because of its statistical similarity to $\overline{\omega_j D(N_2 N_j)/Dt} \times \delta_m^2/S_L^2$.

It is evident from Figs. 9(a)-9(e) that the relative magnitude of baroclinic torque term T_V with respect to the magnitude of viscous dissipation term T_{III} increases with decreasing Le . Figures 9(a)-9(e) further reveal that the vortex-stretching and viscous dissipation terms remain the leading order contributors in all cases considered here but the dilatation and baroclinic terms play leading order roles only in the low Le flames (e.g., $Le = 0.34$ and 0.6 cases considered here). Furthermore, it has been found that the magnitudes of the normalised values of the terms $T_I, T_{II}, T_{III}, T_{IV}$, and T_V decrease with increasing Le .

Equation (4) can be rewritten as

$$\underbrace{\frac{\partial \bar{\Omega}}{\partial t} + \bar{u}_k \frac{\partial \bar{\Omega}}{\partial x_k}}_{\frac{D\bar{\Omega}}{Dt}} = \underbrace{\overline{\omega_i \omega_k \frac{\partial u_i}{\partial x_k}}}_{T_I} - \underbrace{\overline{\epsilon_{ijk} \omega_i \frac{1}{\rho^2} \frac{\partial \rho}{\partial x_j} \frac{\partial \tau_{kl}}{\partial x_l}}}_{T_{II}} + \underbrace{\overline{\frac{\epsilon_{ijk} \omega_i}{\rho} \frac{\partial^2 \tau_{kl}}{\partial x_j \partial x_l}}}_{T_{III}} - \underbrace{2 \overline{\frac{\partial u_k}{\partial x_k} \Omega}}_{T_{IV}} + \underbrace{\overline{\epsilon_{ijk} \frac{\omega_i}{\rho^2} \frac{\partial \rho}{\partial x_j} \frac{\partial p}{\partial x_k}}}_{T_V} - \underbrace{\overline{u'_k \frac{\partial \Omega'}{\partial x_k}}}_{T_{VI}}, \quad (6a)$$

where $\bar{D}(\cdot)/\bar{D}t = \partial(\cdot)/\partial t + \bar{u}_k \partial(\cdot)/\partial x_k$ is the material derivative associated with the mean flow. The last term on the right hand side can be rewritten as

$$\underbrace{-\overline{u'_k \frac{\partial \Omega'}{\partial x_k}}}_{T_{VI}} = - \underbrace{\frac{\partial (\bar{u}'_k \Omega')}{\partial x_k}}_{T_{VI(i)}} + \underbrace{\overline{\Omega' \frac{\partial u'_k}{\partial x_k}}}_{T_{VI(ii)}}. \quad (6b)$$

The normalised values of $(T_I + T_{II} + T_{III} + T_{IV} + T_V)$, T_{VI} , $T_{VI(i)}$, and $T_{VI(ii)}$ for all cases are shown in Figs. 10(a)-10(e). Figure 10(a) indicates that the behaviour of T_{VI} is principally determined by $T_{VI(ii)}$. It is evident from Fig. 10 that $T_{VI(ii)}$ remains positive for cases with small Le , i.e., flame normal acceleration gives rise to positive correlation between fluctuations of enstrophy and dilatation rate, and this term plays an increasingly important role for flames with small values of Le (e.g., $Le = 0.34$ and 0.6 cases considered here). The term $T_{VI(ii)}$ partially eclipses the sink contribution of the dilatation term T_{IV} in flames with small values of Le (e.g., $Le = 0.34$ and 0.6 cases considered here). The fluctuations of enstrophy and dilatation rate are not strongly correlated in flames with $Le \approx 1.0$ and thus the term $T_{VI(ii)}$ assumes small magnitude throughout the flame brush. Figure 10(a) further indicates that the net contribution of $(T_I + T_{II} + T_{III} + T_{IV} + T_V + T_{VI})$ assumes positive values in some locations within the flame brush for the $Le = 0.34$ case. By contrast, $(T_I + T_{II} + T_{III} + T_{IV} + T_V + T_{VI})$ assumes predominantly negative values within the flame brush for the $Le = 0.6, 0.8, 1.0$, and 1.2 cases. This suggests that a fluid particle moving with the mean flow from unburned to burned gas side experiences a monotonic drop of $\bar{\Omega}$ (i.e., $D\bar{\Omega}/Dt < 0$) for the $Le = 0.6, 0.8, 1.0$, and 1.2 flames, whereas the fluid particle moving with mean flow locally experiences an increase in $\bar{\Omega}$ (i.e., $D\bar{\Omega}/Dt > 0$) for the $Le = 0.34$ flame. This is consistent with the observations from Fig. 2(a) which show a decay of $(\omega_i \omega_i)^{1/2} \times \delta_{th}/S_L$ from unburned to burned gas side of the flame brush in the $Le = 0.6, 0.8, 1.0$, and 1.2 flames, but $(\omega_i \omega_i)^{1/2} \times \delta_{th}/S_L$ increases within the flame brush for the $Le = 0.34$ flame.

V. CONCLUSIONS

The effects of Lewis number Le on the transport of vorticity and enstrophy within the flame brush have been analysed using DNS data of freely propagating statistically planar turbulent premixed flames with Le ranging from 0.34 to 1.2 . The investigated flames propagate in intense small-scale turbulence, characterized by $Ka > 1$ and $Da \sim O(1)$, and are associated with the thin reaction zones regime of premixed turbulent combustion. It has been found that, under conditions of the present study, enstrophy decreases significantly from the unburned to the burned gas side of the flame brush in the $Le \approx 1.0$ flames. However, a considerable amount of enstrophy augmentation within the flame brush has been observed for the $Le = 0.34$ case and a similar, but less pronounced behaviour has been observed in the $Le = 0.6$ case. The vorticity components have been shown to exhibit anisotropic behaviour within the flame brush and the extent of anisotropy increases with decreasing Le . It has been demonstrated that the baroclinic torque term is principally responsible for this anisotropic behaviour. The vortex stretching and viscous dissipation terms have been found to be the leading order contributors to the enstrophy transport for all cases; however, the baroclinic torque and the sink term due to dilatation play an increasingly important role for small values of Le . In the case of a low Le , it has been demonstrated that the correlation between the fluctuations of enstrophy and dilatation rate plays an important role in determining the material derivative of enstrophy based on mean flow. The

qualitative nature of the findings of the current paper is unlikely to be modified in the presence of detailed chemistry, but three-dimensional DNS data for high values of turbulent Reynolds number are definitely required for deeper understanding of enstrophy transport in premixed turbulent flames. Furthermore, the present analysis does not address the near wall effects on vorticity dynamics in turbulent reacting flows, which are likely to have significant influences on the vorticity transformation mechanisms discussed in this paper. Some of the aforementioned issues will form the basis of future investigations in this regard.

ACKNOWLEDGMENTS

The first two authors (N.C. and I.K.) are grateful to EPSRC and N8/ARCHER for financial and computational support, respectively. The third author (A.L.) is grateful to Chalmers Transport Area of Advance for financial support.

APPENDIX A: NON-DIMENSIONAL FORM OF CONSERVATION EQUATIONS

The non-dimensional mass, momentum, energy, and progress variable transport equations are presented below,

$$\frac{\partial \rho^+}{\partial t^+} + \frac{\partial(\rho^+ u_i^+)}{\partial x_i^+} = 0, \quad (\text{A1})$$

$$\frac{\partial(\rho^+ u_i^+)}{\partial t^+} + \frac{\partial(\rho^+ u_k^+ u_i^+)}{\partial x_k^+} = -\frac{\partial P^+}{\partial x_i^+} + \frac{1}{Re} \frac{\partial(\tau_{ki}^+)}{\partial x_k^+}, \quad (\text{A2})$$

$$\begin{aligned} \frac{\partial(\rho^+ E^+)}{\partial t^+} + \frac{\partial(\rho^+ u_k^+ E^+)}{\partial x_k^+} = & -(\gamma - 1)Ma^2 \frac{\partial(P^+ u_k^+)}{\partial x_k^+} + \frac{1}{Re}(\gamma - 1)Ma^2 \frac{\partial(\tau_{ki}^+ u_i^+)}{\partial x_k^+} \\ & + \frac{\tau}{Re Pr} \frac{\partial}{\partial x_k^+} \left[\lambda^+ \frac{\partial T^+}{\partial x_k^+} \right] - \frac{\tau}{Re Pr} \frac{\partial}{\partial x_k^+} \left[\rho^+ D^+ \frac{\partial c}{\partial x_k^+} \right], \end{aligned} \quad (\text{A3})$$

$$\frac{\partial(\rho^+ c)}{\partial t^+} + \frac{\partial(\rho^+ u_k^+ c)}{\partial x_k^+} = \dot{w}^+ + \frac{1}{Re Sc} \frac{\partial}{\partial x_k^+} \left[\rho^+ D^+ \frac{\partial c}{\partial x_k^+} \right], \quad (\text{A4})$$

where the non-dimensional quantities are given by

$$\begin{aligned} x_i^+ = x_i/L_{ref}, \quad u_i^+ = u_i/u_{ref}, \quad P^+ = P/\rho_{ref}u_{ref}^2, \quad \tau_{ki}^+ = \tau_{ki}/\rho_{ref}u_{ref}^2, \quad E^+ = E/C_p T_0, \quad (\text{A5}) \\ \dot{w}^+ = \dot{w}L_{ref}/\rho_{ref}u_{ref}, \quad \rho^+ = \rho/\rho_{ref}, \quad \lambda^+ = \lambda/\lambda_{ref}, \quad D^+ = D/D_{ref}, \quad Le = \lambda_{ref}/\rho_{ref}D_{ref}, \end{aligned}$$

with P is the pressure, $E = C_v T + u_k u_k / 2 + H(1 - c)$ is the specific internal energy, and H is the heat of reaction per unit mass of reactants consumed. Therefore,

$$E^+ = \frac{1}{\gamma}(1 + \tau T^+) + \frac{1}{2}(\gamma - 1)Ma^2 u_k^+ u_k^+ + \tau(1 - c). \quad (\text{A6})$$

In Eqs. (A1)-(A4), $Re = \rho_{ref}u_{ref}L_{ref}/\mu_{ref}$ is the nominal Reynolds number, $Ma = u_{ref}/a_{ref}$ is the Mach number, $\gamma = C_p/C_v$ is the ratio of specific heats, Pr is the Prandtl number, and $Sc = Pr \cdot Le$ is the Schmidt number with ρ_{ref} , λ_{ref} , D_{ref} , u_{ref} , L_{ref} , a_{ref} , and μ_{ref} are the reference values of density, thermal conductivity, mass diffusivity, velocity scale, length scale, acoustic velocity, and viscosity, respectively. Here the density, thermal conductivity, mass diffusivity, viscosity, and acoustic speed of the unburned gas are taken to be ρ_{ref} , λ_{ref} , D_{ref} , μ_{ref} , and a_{ref} , respectively, while S_L and $10\delta_{th}$ are considered to be u_{ref} and L_{ref} , respectively. The gas is assumed to follow the ideal gas law $P = \rho R \hat{T}$ which takes the following non-dimensional form:

$$P^+ = \frac{1}{\gamma Ma^2} \rho(1 + \tau T). \quad (\text{A7})$$

Equations (A1)-(A4) are solved in conjunction with Eq. (A7) in the compressible DNS code called SENGAs.⁵⁶ Interested readers are referred to Ref. 56 for further information. It can be seen from

Eq. (A4) that Le comes into play directly through the species conservation equation, which involves $Sc = Pr \cdot Le$. The effects of Le are reflected in the density and pressure gradient fields which in turn affect the vorticity transport.

APPENDIX B: DECOMPOSITION OF VORTICITY TRANSPORT EQUATION

The vorticity transport equation (i.e., Eq. (2)) can be written in the following form:

$$\frac{D\omega_i}{Dt} = K_i, \quad (\text{B1})$$

where

$$K_i = \underbrace{\omega_k \frac{\partial u_i}{\partial x_k}}_{t_{1i}} - \underbrace{\epsilon_{ijk} \frac{1}{\rho^2} \frac{\partial \rho}{\partial x_j} \frac{\partial \tau_{kl}}{\partial x_l}}_{t_{21i}} + \underbrace{\frac{\epsilon_{ijk}}{\rho} \frac{\partial^2 \tau_{kl}}{\partial x_j \partial x_l}}_{t_{22i}} - \underbrace{\omega_i \frac{\partial u_k}{\partial x_k}}_{t_{3i}} + \underbrace{\frac{\epsilon_{ijk}}{\rho^2} \frac{\partial \rho}{\partial x_j} \frac{\partial p}{\partial x_k}}_{t_{4i}}. \quad (\text{B2})$$

Equations (B1) and (B2) can be manipulated as follows. On the one hand,

$$\frac{D\omega_i}{Dt} = \frac{D(\omega_j N_j N_i)}{Dt} + \frac{D(\omega_i - \omega_j N_j N_i)}{Dt} = \frac{D\omega_n}{Dt} + \frac{D\omega_t}{Dt} \quad (\text{B3})$$

and

$$K_i = N_i N_j K_j + (K_i - K_j N_i N_j) = K_n + K_t, \quad (\text{B4})$$

and therefore, one can write the following:

$$\frac{D\omega_i}{Dt} = \frac{D\omega_n}{Dt} + \frac{D\omega_t}{Dt} = K_n + K_t. \quad (\text{B5})$$

It is worth stressing, however, that $D\omega_n/Dt \neq N_i N_j K_j$ and $D\omega_t/Dt \neq (K_i - K_j N_i N_j)$, i.e., $D\omega_n/Dt \neq K_n$ and $D\omega_t/Dt \neq K_t$.

On the other hand,

$$N_i N_j \frac{D\omega_j}{Dt} = N_i N_j K_j = K_n$$

and

$$\frac{D\omega_i}{Dt} - N_i N_j \frac{D\omega_j}{Dt} = K_i - K_j N_i N_j = K_t. \quad (\text{B6})$$

Therefore,

$$\frac{D(\omega_n)}{Dt} = \frac{D(\omega_j N_j N_i)}{Dt} = N_j N_i \frac{D\omega_j}{Dt} + \omega_j \frac{D(N_j N_i)}{Dt} = K_n + \omega_j \frac{D(N_j N_i)}{Dt}, \quad (\text{B7})$$

$$\frac{D\omega_t}{Dt} = \frac{D(\omega_i - \omega_j N_j N_i)}{Dt} = \frac{D\omega_i}{Dt} - N_j N_i \frac{D\omega_j}{Dt} - \omega_j \frac{D(N_j N_i)}{Dt} = K_t - \omega_j \frac{D(N_j N_i)}{Dt}. \quad (\text{B8})$$

The variations of $\overline{\omega_j D(N_1 N_j)/Dt}$ and $\overline{\omega_j D(N_2 N_j)/Dt}$ ($\overline{\omega_j D(N_3 N_j)/Dt}$ is statistically similar to $\overline{\omega_j D(N_2 N_j)/Dt}$ and is thus not explicitly shown here) with \tilde{c} for all cases considered here are presented in Fig. 11. It can be seen from Figs. 11 and 5 that the magnitude of $\overline{\omega_j D(N_i N_j)/Dt}$ remains much smaller than the magnitudes of the leading order terms of $(t_{qn} t_{qn})^{1/2}$, e.g., $(t_{22n} t_{22n})^{1/2}$. Accordingly, the magnitudes of the terms of the conservation equation of $\overline{N_i N_j \omega_j}$ are expected to be close to those of $(t_{qn} t_{qn})^{1/2} = \left((t_q \cdot \vec{N})^2 \right)^{1/2}$, where $q = 1, 21, 22, 3$, and 4.

¹ H. Tennekes and J. L. Lumley, *A First Course in Turbulence*, 1st ed. (MIT Press, Cambridge, Massachusetts, USA, 1972).

² S. B. Pope, *Turbulent Flows*, 1st ed. (Cambridge University Press, Cambridge, UK, 2000).

³ P. A. Durbin and B. A. Petterson Reif, *Statistical Theory and Modeling for Turbulent Flows*, 2nd ed. (Wiley, 2010).

⁴ B. Karlovitz, D. W. Denniston, and F. E. Wells, "Investigation of turbulent flames," *J. Chem. Phys.* **19**, 541 (1951).

- ⁵ P. A. Libby and K. N. C. Bray, "Counter gradient diffusion in premixed turbulent flames," *AIAA J.* **19**, 205 (1981).
- ⁶ J. B. Moss, "Simultaneous measurements of concentration and velocity in an open premixed turbulent flame," *Combust. Sci. Technol.* **22**, 119 (1980).
- ⁷ A. N. Lipatnikov and J. Chomiak, "Effects of premixed flames on turbulence and turbulent scalar transport," *Prog. Energy Combust. Sci.* **36**, 1 (2010).
- ⁸ K. K. Nomura and S. E. Elghobashi, "The structure of inhomogeneous turbulence in variable density nonpremixed flames," *Theor. Fluid Dyn.* **5**, 153 (1993).
- ⁹ O. N. Boratov, S. E. Elghobashi, and R. Zhong, "On the alignment of strain, vorticity and scalar gradient in turbulent, buoyant, nonpremixed flames," *Phys. Fluids* **10**(9), 2260 (1996).
- ¹⁰ F. A. Jaberi, D. Livescu, and C. K. Madnia, "Characteristics of chemically reacting compressible homogeneous turbulence," *Phys. Fluids* **12**(5), 1189 (2000).
- ¹¹ P. E. Hamlington, A. Y. Poludnenko, and E. S. Oran, "Interactions between turbulence and flames in premixed reacting flows," *Phys. Fluids* **23**, 125111 (2011).
- ¹² T. C. Truermiet, F. T. M. Nieuwstadt, and B. J. Boersma, "Direct numerical simulation of homogeneous turbulence in combination with premixed combustion at low Mach number modelled by the G-equation," *J. Fluid Mech.* **565**, 25 (2006).
- ¹³ A. N. Lipatnikov, S. Nishiki, and T. Hasegawa, "A direct numerical study of vorticity transformation in weakly turbulent premixed flames," *Phys. Fluids* **26**, 105104 (2014).
- ¹⁴ A. M. Steinberg, J. F. Driscoll, and S. L. Ceccio, "Measurements of turbulent premixed flame dynamics using cinema stereoscopic PIV," *Exp. Fluids* **44**, 985 (2008).
- ¹⁵ A. M. Steinberg and J. F. Driscoll, "Straining and wrinkling processes during turbulence-premixed flame interaction measured using temporally-resolved diagnostics," *Combust. Flame* **156**, 2285 (2009).
- ¹⁶ A. M. Steinberg, J. F. Driscoll, and S. L. Ceccio, "Three-dimensional temporally resolved measurements of turbulence-flame interactions using orthogonal-plane cinema-stereoscopic PIV," *Exp. Fluids* **47**, 527 (2009).
- ¹⁷ A. M. Steinberg, J. F. Driscoll, and S. L. Ceccio, "Temporal evolution of flame stretch due to turbulence and the hydrodynamic instability," *Proc. Combust. Inst.* **32**, 1713 (2009).
- ¹⁸ N. Chakraborty, "Statistics of vorticity alignment with local strain rates in turbulent premixed flames," *Eur. J. Mech. B/Fluids* **46**, 201 (2014).
- ¹⁹ E. D. Siggia, "Numerical study of small scale intermittency in three-dimensional turbulence," *J. Fluid Mech.* **107**, 375 (1981).
- ²⁰ W. T. Ashurst, A. Kerstein, R. M. Kerr, and C. H. Gibson, "Alignment of vorticity and scalar gradient with strain rate in simulated Navier-Stokes turbulence," *Phys. Fluids A* **30**, 2343 (1987).
- ²¹ Z.-S. She, E. Jackson, and S. Orszag, "Structure and dynamics of homogeneous turbulence: Models and simulations," *Proc. R. Soc. A* **434**, 101 (1991).
- ²² A. J. Majda, "Vorticity, turbulence, and acoustics in fluid flow," *SIAM Rev.* **33**, 349 (1991).
- ²³ J. Jimenez, "Kinematic alignment effects in turbulent flows," *Phys. Fluids A* **4**, 652 (1992).
- ²⁴ A. Tsinober, E. Kit, and T. Dracos, "Experimental investigation of the field of velocity gradients in turbulent flows," *J. Fluid Mech.* **242**, 169 (1992).
- ²⁵ B. W. Zeff, D. D. Lanterman, R. McAllister, R. Roy, E. J. Kostelich, and D. P. Lathrop, "Measuring intense rotation and dissipation in turbulent flows," *Nature* **421**, 146 (2003).
- ²⁶ B. Lüthi, A. Tsinober, and W. Kinzelbach, "Lagrangian measurement of vorticity dynamics in turbulent flow," *J. Fluid Mech.* **528**, 87 (2005).
- ²⁷ P. E. Hamlington, J. Schumacher, and W. J. A. Dahm, "Local and nonlocal strain rate and vorticity alignment in turbulent flows," *Phys. Rev. E* **77**, 026303 (2008).
- ²⁸ H. Xu, A. Pumir, and E. Bodenschatz, "The pirouette effect in turbulent flows," *Nat. Phys.* **7**, 709 (2011).
- ²⁹ M. Mizomoto, S. Asaka, S. Ikai, and C. K. Law, "Effects of preferential diffusion on the burning intensity of curved flames," *Proc. Combust. Inst.* **20**, 1933 (1984).
- ³⁰ C. K. Law, *Combustion Physics* (Cambridge University Press, Cambridge, UK, 2010).
- ³¹ C. K. Law and O. C. Kwon, "Effects of hydrocarbon substitution on atmospheric hydrogen-air flame propagation," *Int. J. Hydrogen Energy* **29**, 867 (2004).
- ³² F. Dinkelacker, B. Manickam, and S. R. Muppala, "Modelling and simulation of lean premixed turbulent methane/hydrogen/air flames with an effective Lewis number approach," *Combust. Flame* **158**, 1742 (2011).
- ³³ G. I. Barenblatt, Y. B. Zeldovich, and A. G. Istratov, "On heat and diffusion effects in stability of laminar flames," *ZhPMTF* **4**, 21 (1962).
- ³⁴ G. I. Sivashinsky, "Diffusional-thermal theory of cellular flames," *Combust. Sci. Technol.* **16**, 137 (1977).
- ³⁵ P. Pelcé and P. Clavin, "Influence of hydrodynamics and diffusion upon the stability limits of laminar premixed flames," *J. Fluid Mech.* **124**, 219 (1982).
- ³⁶ M. Matalon and B. J. Matkowsky, "Flames as gas dynamic discontinuities," *J. Fluid Mech.* **124**, 239 (1982).
- ³⁷ K. Wohl and L. Shore, "Experiments with butane-air and methane-air flames," *Ind. Eng. Chem.* **47**, 828 (1955).
- ³⁸ V. P. Karpov and E. S. Severin, "Effects of molecular-transport coefficients on the rate of turbulent combustion," *Combust., Explos. Shock Waves* **16**, 41 (1980).
- ³⁹ R. G. Abdel-Gayed, D. Bradley, M. Hamid, and M. Lawes, "Lewis number effects on turbulent burning velocity," *Proc. Combust. Inst.* **20**, 505 (1984).
- ⁴⁰ H. Kido, T. Kitagawa, K. Nakashima, and K. Kato, "An improved model of turbulent mass burning velocity," *Memoirs Faculty Eng. Kyushu Univ.* **49**, 229 (1989).
- ⁴¹ M. S. Wu, A. Kwon, G. Driscoll, and G. M. Faeth, "Turbulent premixed hydrogen/air flames at high Reynolds numbers," *Combust. Sci. Tech.* **73**, 327 (1990).
- ⁴² B. Renou, A. Boukhalfa, D. Peuchberty, and M. Trinité, "Effects of stretch on the local structure of freely propagating premixed low-turbulent flames with various Lewis numbers," *Proc. Combust. Inst.* **27**, 841 (1998).
- ⁴³ P. Venkateswaran, A. Marshall, D. H. Shin, D. Noble, J. Seitzman, and T. Lieuwen, "Measurements and analysis of turbulent consumption speeds of H₂/CO mixtures," *Combust. Flame* **158**, 1602 (2011).

- ⁴⁴ W. T. Ashurst, N. Peters, and M. D. Smooke, "Numerical simulation of turbulent flame structure with non-unity Lewis number," *Combust. Sci. Technol.* **53**, 339 (1987).
- ⁴⁵ D. C. Haworth and T. J. Poinso, "Numerical simulations of Lewis number effects in turbulent premixed flames," *J. Fluid Mech.* **244**, 405 (1992).
- ⁴⁶ C. J. Rutland and A. Trouvé, "Direct simulations of premixed turbulent flames with nonunity Lewis numbers," *Combust. Flame* **94**, 41 (1993).
- ⁴⁷ A. Trouvé and T. J. Poinso, "The evolution equation for flame surface density in turbulent premixed combustion," *J. Fluid Mech.* **278**, 1 (1994).
- ⁴⁸ N. Chakraborty and R. S. Cant, "Influence of Lewis number on curvature effects in turbulent premixed flame propagation in the thin reaction zones regime," *Phys. Fluids* **17**, 105105 (2005).
- ⁴⁹ I. Han and K. H. Huh, "Roles of displacement speed on evolution of flame surface density for different turbulent intensities and Lewis numbers for turbulent premixed combustion," *Combust. Flame* **152**, 194 (2008).
- ⁵⁰ N. Chakraborty and M. Klein, "Influence of Lewis number on the surface density function transport in the thin reaction zones regime for turbulent premixed flames," *Phys. Fluids* **20**, 065102 (2008).
- ⁵¹ N. Chakraborty and R. S. Cant, "Effects of Lewis number on turbulent scalar transport and its modelling in turbulent premixed flames," *Combust. Flame* **156**, 1427 (2009).
- ⁵² N. Chakraborty, M. Katragadda, and R. S. Cant, "Effects of Lewis number on turbulent kinetic energy transport in turbulent premixed combustion," *Phys. Fluids* **23**, 075109 (2011).
- ⁵³ A. J. Aspden, M. S. Day, and J. B. Bell, "Characterization of low Lewis number flames," *Proc. Combust. Inst.* **33**, 1463 (2011).
- ⁵⁴ V. R. Kuznetsov and V. A. Sabelnikov, *Turbulence and Combustion* (Hemisphere Publishing Corporation, New York, 1990).
- ⁵⁵ A. N. Lipatnikov and J. Chomiak, "Molecular transport effects on turbulent flame propagation and structure," *Prog. Energy Combust. Sci.* **31**, 1 (2005).
- ⁵⁶ K. W. Jenkins and R. S. Cant, "DNS of turbulent flame kernels," in *Proceedings of 2nd AFOSR Conference on DNS and LES* (Kluwer Academic Publishers, Dordrecht, 1999), p. 192.
- ⁵⁷ A. A. Wray, "Minimal storage time advancement schemes for spectral methods," Report No. MS 202 A-1, NASA Ames Research Center, California, 1990.
- ⁵⁸ R. S. Rogallo, "Numerical experiments in homogeneous turbulence," NASA Technical Memorandum 91416, NASA Ames Research Center, California, 1981.
- ⁵⁹ G. K. Batchelor and A. A. Townsend, "Decay of turbulence in the final period," *Proc. R. Soc. A* **194**, 527 (1948).
- ⁶⁰ N. Peters, *Turbulent Combustion, Cambridge Monograph on Mechanics* (Cambridge University Press, Cambridge, 2000).
- ⁶¹ D. Veynante, A. Trouvé, K. N. C. Bray, and T. Mantel, "Gradient and counter-gradient turbulent scalar transport in turbulent premixed flames," *J. Fluid Mech.* **332**, 263 (1997).
- ⁶² M. Boger, D. Veynante, H. Boughanem, and A. Trouvé, "Direct numerical simulation analysis of flame surface density concept for large eddy simulation of turbulent premixed combustion," *Proc. Combust. Inst.* **27**, 917 (1998).
- ⁶³ F. Charlette, C. Meneveau, and D. Veynante, "A power-law flame wrinkling model for LES of premixed turbulent combustion. Part I: Nondynamic formulation and initial tests," *Combust. Flame* **131**, 181 (2002).
- ⁶⁴ R. Grout, "An age extended progress variable for conditioned reaction rates," *Phys. Fluids* **19**, 105107 (2007).
- ⁶⁵ I. Han and K. H. Huh, "Effects of Karlovitz number on the evolution of the flame surface density in turbulent premixed flames," *Proc. Combust. Inst.* **32**, 1419 (2009).
- ⁶⁶ C. Pera, S. Chevillard, and J. Reveillon, "Effects of residual burnt gas heterogeneity on early flame propagation and on cyclic variability in spark-ignited engines," *Combust. Flame* **160**, 1020 (2013).
- ⁶⁷ C. Dopazo, L. Cifuentes, J. Martin, and C. Jimenez, "Strain rates normal to approaching iso-scalar surfaces in a turbulent premixed flame," *Combust. Flame* **162**, 1729 (2014).
- ⁶⁸ F. A. Williams, *Combustion Theory*, 2nd ed. (Benjamin/Cummings, Menlo Park, CA, 1985).
- ⁶⁹ Ya. B. Zeldovich, G. I. Barenblatt, V. B. Librovich, and G. M. Makhviladze, *The Mathematical Theory of Combustion and Explosions* (Plenum Publishing Corporation, New York, 1985).
- ⁷⁰ P. Clavin, "Dynamics of combustion fronts in premixed gases: From flames to detonations," *Proc. Combust. Inst.* **28**, 569 (2000).
- ⁷¹ G. I. Sivashinsky, "Some developments in premixed combustion modeling," *Proc. Combust. Inst.* **29**, 1737 (2002).
- ⁷² M. Matalon, "Flame dynamics," *Proc. Combust. Inst.* **32**, 57 (2009).
- ⁷³ A. G. Istratov and V. B. Librovich, "On the stability of gasdynamic discontinuities associated with chemical reactions. The case of a spherical flame," *Astronaut. Acta* **14**, 453 (1969).
- ⁷⁴ J. K. Bechtold and M. Matalon, "Hydrodynamic and diffusion effects on the stability of spherically expanding flames," *Combust. Flame* **67**, 77 (1987).
- ⁷⁵ R. Addabo, J. K. Bechtold, and M. Matalon, "Wrinkling of spherically expanding flames," *Proc. Combust. Inst.* **29**, 1527 (2002).
- ⁷⁶ M. Matalon, C. Cui, and J. K. Bechtold, "Hydrodynamic theory of premixed flames: Effects of stoichiometry, variable transport coefficients and arbitrary reaction orders," *J. Fluid Mech.* **487**, 179 (2003).
- ⁷⁷ A. G. Class, B. J. Matkowsky, and A. Y. Klimenko, "A unified model of flames as gasdynamic discontinuities," *J. Fluid Mech.* **491**, 11 (2003).
- ⁷⁸ A. G. Class, B. J. Matkowsky, and A. Y. Klimenko, "Stability of planar flames as gasdynamic discontinuities," *J. Fluid Mech.* **491**, 51 (2003).
- ⁷⁹ A. P. Kelley, J. K. Bechtold, and C. K. Law, "Premixed flame propagation in a confining vessel with weak pressure rise," *J. Fluid Mech.* **691**, 26 (2012).
- ⁸⁰ V. A. Sabelnikov and A. N. Lipatnikov, "Transition from pulled to pushed fronts in premixed turbulent combustion: Theoretical and numerical study," *Combust. Flame* **162**, 2893 (2015).
- ⁸¹ K. N. C. Bray, P. A. Libby, and J. B. Moss, "Unified modelling approach for premixed turbulent combustion. Part I: General formulation," *Combust. Flame* **61**, 87 (1985).